Elsevier Editorial System(tm) for Nuclear Inst. and Methods in Physics Research, A
Manuscript Draft

Manuscript Number: NIMA-D-19-00217R3

Title: Development of an alpha-particle imaging detector based on a low radioactivity micro-time-projection chamber

Article Type: Full length article

Section/Category: Space Radiation and Underground Detectors

Keywords: Alpha-particle detector; Position sensitivity; Time projection; chamber; ¥mu$-PIC; Low background

Corresponding Author: Dr. Hiroshi Ito,

Corresponding Author's Institution: ICRR, University of Tokyo

First Author: Hiroshi Ito

Order of Authors: Hiroshi Ito; Takashi Hashimoto, Ph. D; Kentaro Miuchi, Ph. D; Kazuyoshi Kobayashi, Ph. D; Yasuo Takeuchi, Ph. D; Kiseki D Nakamura, Ph. D; Tomonori Ikeda; Hirohisa Ishiura

Abstract: An important issue for rare-event-search experiments, such as the search for dark matter or neutrinoless double beta decay, is to reduce radioactivity of the detector materials and the experimental environment. The selection of materials with low radioactive impurities, such as isotopes of the uranium and thorium chains, requires a precise measurement of surface and bulk radioactivity. Focused on the first one, an alpha-particle detector has been developed based on a gaseous micro-time-projection chamber. A low-$¥alpha$ $¥mu$-PIC with reduced alpha-emission background was installed in the detector. The detector offers the advantage of position sensitivity, which allows the alpha-particle contamination of the sample to be imaged and the background to be measured at the same time. The detector performance was measured by using an alpha-particle source. The measurement with a sample was also demonstrated and the sensitivity is discussed.

*Manuscript
Click here to view linked References

Development of an alpha-particle imaging detector based on a low radioactivity micro-time-projection chamber

H. Ito[a*], T. Hashimoto[a], K. Miuchi[a], K. Kobayashi[b,c], Y. Takeuchi[a,c], K. D. Nakamura[a], T. Ikeda[a], and H. Ishiura[a]

[a] *Kobe University, Kobe, Hyogo 657-8501, Japan.*

[b] *Institute for Cosmic Ray Research (ICRR), the University of Tokyo, Kashiwa, Chiba 277-8582 Japan.*

[c] *Kavli Institute for the Physics and Mathematics of the Universe (WPI), The University of Tokyo Institutes for Advanced Study, University of Tokyo, Kashiwa, Chiba 277-8583, Japan.*

Abstract

An important issue for rare-event-search experiments, such as the search for dark matter or neutrinoless double beta decay, is to reduce radioactivity of the detector materials and the experimental environment. The selection of materials with low radioactive impurities, such as isotopes of the uranium and thorium chains, requires a precise measurement of surface and bulk radioactivity. Focused on the first one, an alpha-particle detector has been developed based on a gaseous micro-time-projection chamber. A low-α μ-PIC with reduced alpha-emission background was installed in the detector. The detector offers the advantage of position sensitivity, which allows the alpha-particle contamination of the sample to be imaged and the background to be measured at the same time. The detector performance was measured by using an alpha-particle source. The measurement with a sample was also demonstrated and the sensitivity is discussed.

Keywords: Alpha-particle detector, Position sensitivity, Time projection chamber, μ-PIC, Low background

1. Introduction

Approximately 27% of the universe is dominated by non-baryonic matter, called dark matter. Although many experimental groups have been searching for dark matter, arguably a direct detection has not been observed. Typical experiments that search for dark matter are performed by using massive, low-background detectors. Although the DAMA group has observed the presumed annual modulation of dark matter particles in the galactic halo with a significance of 9.3σ [1], other groups such as XENON1T [2] and LUX [3] were unable to confirm these results. Meanwhile, a direction-sensitive method has been focused because of an expected clear anisotropic signal due to the motion of the solar system in the galaxy [4]. The NEWAGE group precedes a three-dimensionally sensitive dark matter search with a micro-time-projection chamber (micro-TPC), being the main background surface alpha particles from ^{238}U and ^{232}Th in the detector materials or in the μ-PIC [5].

Neutrinoless double beta ($0\nu\beta\beta$) decay is a lepton-number-violating process, which suggests the neutrino as a Majorana particle (i.e. it is its own antiparticle). Experiments like GERDA [6] and KamLAND-Zen [7] have been able to set a lower limit on the half-life over 10^{25} yr and 10^{26} yr at 90%CL by using ^{76}Ge and ^{136}Xe, respectively, but no positive signal of the $0\nu\beta\beta$ process has been observed yet. Conversely, a tracking system for two electrons provides strong evidence of the $0\nu\beta\beta$ decay process. The $0\nu\beta\beta$ background has been well investigated as radioactive impurities such as ^{238}U and ^{232}Th decay-chain isotopes, ^{40}K, ^{60}Co, ^{137}Cs including in the detector material, which emit γ with around MeV [8, 9]. The NEMO3 group set lower limits at

*Corresponding author. E-mail address: ito.hiroshi@crystal.kobe-u.ac.jp (H. Ito).

$T_{1/2}(0\nu\beta\beta) > 2.5 \times 10^{23}$ yr (90%CL) for ^{82}Se [10], and $T_{1/2}(0\nu\beta\beta) > (1.1 - 3.2) \times 10^{21}$ yr (90%CL) for ^{150}Nd [11]. For this experiment background is dominated by the ^{208}Tl and ^{214}Bi contamination present in the double beta emitter source foils. The SuperNEMO group has developed the BiPo-3 detector to measure the radioactive impurities in these foils with a sensitivity less than 2 μBq/kg (90%CL) for ^{208}Tl and 140 μBq/kg (90%CL) for ^{214}Bi [12]. Therefore, the background of $0\nu\beta\beta$ decay is not only a contamination by the end point of continuous energy in an ordinary $2\nu\beta\beta$ decay process, but also the radiative impurities such as ^{238}U and ^{232}Th in the detector.

To estimate the radioactive impurities in the detector materials, the XMASS group measured ^{210}Pb and ^{210}Po in the bulk of copper by using a commercial alpha-particle detector (Ultra-Lo 1800, XIA) [13]. The alpha detector has a good energy resolution (as explained in Sec. 3.2) and a mechanism to reduce the background by waveform analysis, and thus its sensitivity is $\sim 10^{-4}$ α/cm^2/hr. However, it has no position sensitivity. A sample such as a micro pattern gas detector board does not have a uniform radioactive contamination. For example the impurities can be in a particular location due to the manufacturing process. Therefore, a position-sensitive alpha detector is required in order to determine the site and perhaps the process associated with the materials contamination.

This paper is organized as follows. The details of the alpha-particle detector, setup, low-α micro pixel chamber (μ-PIC), gas circulation system, electronics, and trigger and data acquisition systems are described in Sec. 2. The performance check that uses the alpha-particle source, a sample test, and background estimation are described in Sec. 3. The remaining background of the detector and future prospects are discussed in Sec. 4. Finally, main conclusions are presented in Sec. 5.

2. Alpha-particle imaging detector based on gaseous micro-TPC

A new alpha-particle detector was developed based on a gaseous micro-TPC upgraded from the NEWAGE-0.3a detector [14] which was used to search for dark matter from September, 2008 to January, 2013. The detector consisted of the micro-TPC using a low-α μ-PIC as readout, a gas circulation system, and electronics, as shown in Fig.1. The TPC was enclosed in a stainless-steel vessel for the gas seal during the measurement.

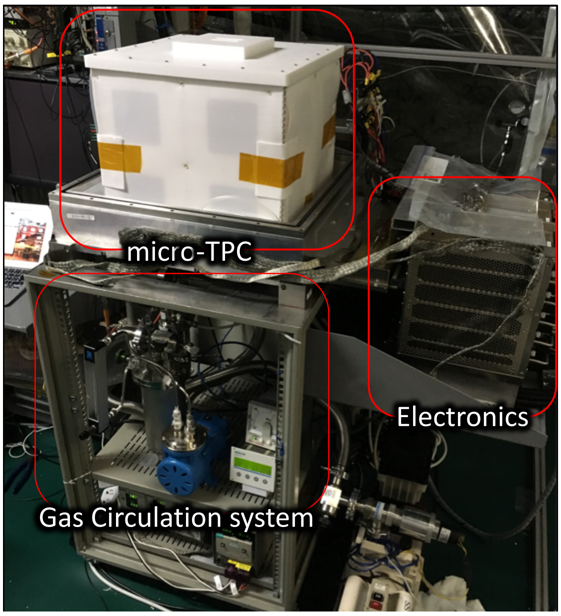

Fig. 1: Photograph of the experimental setup. The detector system is composed of a micro-TPC, a gas circulation system, and electronics. The stainless-steel vessel is uncovered so that the outer view of the TPC field cage can be viewed.

2.1. Setup and configuration

Figure 2 shows a schematic view of the detector, where the gas volume is (35 cm $\times$ 35 cm) $\times$ 31 cm. The detector was placed underground at the Kamioka facility in the Institute for Cosmic Ray Research, Japan. An oxygen-free copper plate with a surface electro-polished to a roughness of 0.4 μm and a size of (35 cm $\times$ 35 cm) $\times$ 0.1 cm was used as the drift plate. The drift plate had an opening with a size of 9.5 cm $\times$ 9.5 cm as a sample window. A copper mesh made of 1-mm-ϕ wire in 1-cm pitch (aperture ratio of 0.81) was set on the drift plate to hold the sample at the window area, as shown in Fig. 3. The electrons ionized by the alpha particles drift towards the μ-PIC with a vertical upward-pointing electric field E. CF_4 gas (TOMOE SHOKAI Co.LTD, 5N grade: a purity of 99.999% or more), which was also used in the NEWAGE-0.3a, was used because of the low diffusion properties. The pressure was set at 0.2 bar as a result of the optimization between the expected track length and the detector stability. The track length was expected to be longer, which improved the tracking performance when the gas pressures were low, while the discharge rate of the μ-PIC increased. The range of 5 MeV alpha particle is $\sim$8 cm in 0.2 bar CF_4 gas, which would provide a reasonable detection efficiency considering the detector size. The electric field in the drift volume, $E = 0.4$ kV/cm/bar, was formed by supplying a negative voltage of 2.5 kV and placing field-shaping patterns with chain resistors every centimeter [15]. The drift velocity was 7.4 ± 0.1 cm/μs. The μ-PIC anode was connected to +550 V. The typical gas gain of μ-PIC was 10^3 at $\sim$ 500 V.

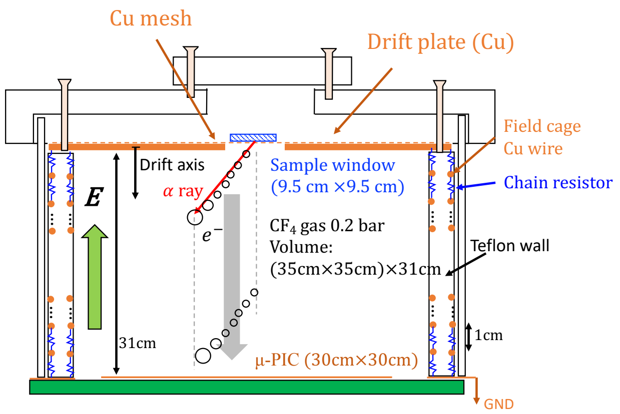

Fig. 2: Schematic cross section of detector setup. Sample window size is 9.5 cm × 9.5 cm. Electric field is formed by a drift plate biased at -2.5 kV and copper wires with 1 cm pitch connecting with chain registers.

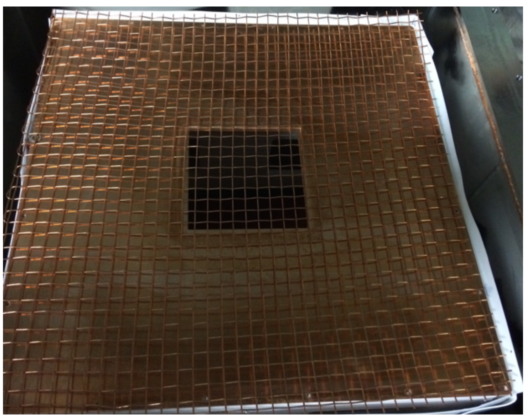

Fig. 3: Drift plate with a sample window (hole size is 9.5 cm × 9.5 cm) and copper support mesh.

2.2. Low-α μ-PIC

The background study for the direction-sensitive dark matter search suggests that μ-PIC has radioactive impurities of ^{238}U and ^{232}Th which emit alpha particles [5]. A survey with a HPGe detector revealed that μ-PIC's glass cloth was the main background source, and so the impurities were removed. The polyimide with glass cloth in the μ-PIC was replaced with a new material of polyimide and epoxy. Details of the device with the new material, a low-α μ-PIC, will be described in Ref [16, 17].

2.3. Gas circulation system

A gas circulation system that uses activated charcoal pellets (Molsievon, X2M4/6M811) was developed for the suppression of radon background and a prevention of gain deterioration due to the outgassing. A pump (EMP, MX-808ST-S) and a needle-type flow-meter (KOFLOC, PK-1250) were used to flow the gas at a rate of $\sim$ 500 cm^3/min. The gas pressure was monitored to ensure the stable operation of the circulation system, operating within $\pm$2% for several weeks.

2.4. Electronics and trigger and data acquisition systems

The electronics for the μ-PIC readout consisted of amplifier-shaper discriminators [18] for 768 anode and 768 cathode signals and a position-encoding module [19] to reconstruct the hit pattern. A data acquisition system consisted of a memory board to record tracks and a flash analog-to-digital converter (ADC) for the energy measurement. The flash ADC with 100 MHz sampling recorded the sum signal of the cathode strips with a full time range of 12 μs. The anode sum signal issued the trigger. The trigger occurred when the electrons closest to the detection plane (indicated with the largest circle (e^-) in Fig. 2) reach the μ-PIC. Since the main purpose of the detector is the alpha particle detection from the sample, the emission position of the alpha particle in the anode-cathode plane was determined at the position most distant from the μ-PIC in the track (the smallest circle in Fig. 2).

3. Performance check

3.1. Alpha-particle source

A 10 cm × 10 cm copper plate with ^{210}Pb accumulated on the surface was used as an alpha-particle source for the energy calibration and energy-resolution measurement [13]. The source emits alpha particles with an energy of 5.3 MeV as a decay of ^{210}Po. The alpha-particle emission rate (hereinafter called the α rate) of the entire source plate was calibrated to be 1.49 ± 0.01 α s^{-1} for 4.8–5.8 MeV by using the Ultra-Lo 1800 [13].

3.2. Energy calibration

An energy calibration was conducted with the alpha-particle source (5.3 MeV). The event's energy was obtained by integrating the charge from the pulses registered by the flash ADC. Thus spectra showed in this paper are presented in MeV. Figure 4 shows a typical energy spectrum of the alpha-particle source. The energy resolution was estimated to be 6.7% (1σ) for 5.3 MeV, which is not as good as the Ultra-Lo 1800 resolution of 4.7% (1σ) for 5.3 MeV. This deterioration was thought to be due to the gain variation of the μ-PIC detection area.

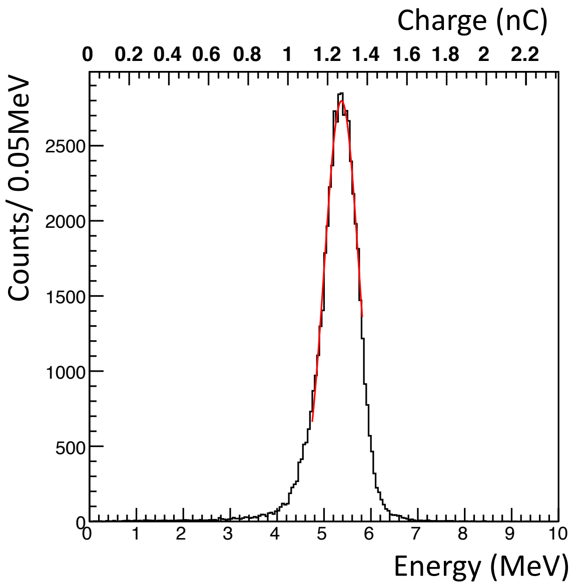

Fig. 4: Energy spectrum for alpha particles from ^{210}Po (5.3 MeV). Red line is a fit result with a Gaussian.

3.3. Event reconstruction

Figure 5 shows a typical event display with the tracks and flash ADC waveform data for alpha-particle emission from ^{210}Po. The hit points were determined based on coincidence of anode and cathode detections. Figure 5 (c) shows the anode-cathode plane for the track. The open circles correspond to hits registered in data. The red solid line is a linear fit result. The dashed line represents the edge of the sample window. The solid blue point is the emission point of the alpha particle. The scheme of the determination of the emission point, or the track sense, is explained in Sec. 3.4. Figure 5 (a) and (d) show anode- and cathode-drift planes, respectively. The drift coordinate is converted from the timing and is set to zero base, which corresponds to the drift-plate position. Figure 5 (b) shows a flash ADC waveform.

The track angles were determined on the anode-cathode, anode-drift, and cathode-drift planes. These angles were determined with a common fitting algorithm. First, the weighted means of the hit points $(x_{\rm w}, y_{\rm w})$ were defined as

$$\begin{pmatrix} x_{\rm w} \\ y_{\rm w} \end{pmatrix} = \frac{1}{n}\sum_{j=0}^{n} \begin{pmatrix} x_j \\ y_j \end{pmatrix}, \qquad (1)$$

where x_j and y_j are the measured hit points and n is the number of points. Next, the track was shifted and rotated through the angle θ as follows

$$\begin{pmatrix} x'_j \\ y'_j \end{pmatrix} = \begin{pmatrix} \cos\theta & -\sin\theta \\ \sin\theta & \cos\theta \end{pmatrix} \begin{pmatrix} x_j - x_{\rm w} \\ y_j - y_{\rm w} \end{pmatrix}. \qquad (2)$$

Here x'_j and y'_j are the points after the shift, the rotation angle θ were determined to minimize the quantity f, which is defined as

$$f(\theta) = \sum y'^2_j, \qquad (3)$$

where this formula means a sum of the square of the distance between the rotated point and the x axis. This method has the advantage to determine the angle with no infinity pole at $\theta = 90°$ (i.e. parallel to cathode strip (fitting in the anode-cathode plane) or drift axis (fitting in the anode-drift and cathode-drift plane)).

3.4. Track-sense determination

Backgrounds in low radioactivity alpha-particle detectors are in general alpha particles from the radon (radon-α) and materials of construction used in the detector (detector-α). The radon-α's are expected to be distributed uniformly in the gas volume with isotropic directions. The detector-α's are expected to have position and direction distributions specific to their sources. One of the main sources of the detector-α's is the μ-PIC so the directions of α's coming from this component are mostly

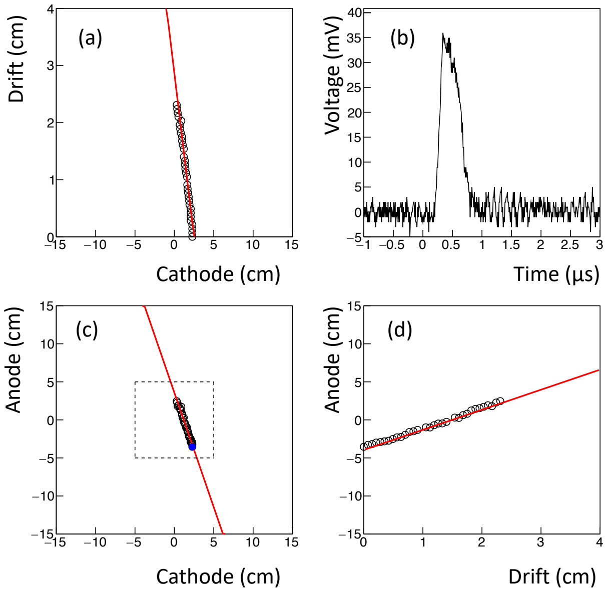

Fig. 5: Event display of an alpha particle from 210Po. (a) cathode-drift projection, (b) flash ADC waveform (c) cathode-anode projection, and (d) anode-drift projection are displayed. The drift coordinate is set to zero base corresponding to the drift plate position for the top of the track.

upward-oriented. Since the direction of alpha particles from the sample are downward, these detector-α's and half of the radon-α's can be rejected by the cut of upward-direction events.

The deposit energy per unit path length, dE/dx of an alpha particle with an initial energy over a few MeV, has a peak before stopping (Bragg peak). The number of electrons ionized by the alpha particle in the gas is proportional to dE/dx, and dE/dx along the track profile is projected onto the time evolution in the signal due to the mechanism of the TPC. This time profile was recorded as the waveform and thus the track sense (i.e., whether the track was upward or downward) can be determined from the waveform.

A parameter to determine the track sense is

$$F_{\rm dwn} = S_2/(S_1 + S_2), \tag{4}$$

where S_1 and S_2 are the time-integrated waveform before and after the peak. They are defined as

$$S_1 = \int_{t_0}^{t_p} v(t)dt, \tag{5}$$

$$S_2 = \int_{t_p}^{t_1} v(t)dt. \tag{6}$$

Here, $t_0 = 0\ \mu$s, $t_1 = 1.5\ \mu$s, and t_p are the start, stop, and peak time, respectively, for the waveform shown in Fig. 5 (b). The t_p is determined as a time when the voltage is highest in the region between t_0 and t_1. Figure 6 (a) shows typical $F_{\rm dwn}$ distribution with the alpha-particle source, where most of the events are expected to be downward-oriented. The $F_{\rm dwn}$ values of the downward events are distributed around 0.7, as shown by the black-shaded histograms. Conversely, radon-α's have an isotropic direction, i.e., $F_{\rm dwn}$ has two components of upward- and downward-oriented, as shown by the red solid histogram, where the radon-α are background events in the sample test data, as explained later. The scale of the source-α was normalized to the radon-α peak of downward for clarity. Figure 6 (b) shows the efficiency related on $F_{\rm dwn}$ threshold for downward-(black solid) and upward-oriented (blue dashed). The selection efficiency of $F_{\rm dwn} > 0.5$ was estimated to be 0.964 ± 0.004 in the source-α spectrum while the radon background was reduced to half. The blue dashed histogram is a spectrum that subtracted the normalized source-α from the radon-α. The cut efficiency of the upward-oriented events ($F_{\rm dwn} \leq 0.5$) was estimated to be 0.85 ± 0.04. The energy dependence of $F_{\rm dwn}$ will be explained in Sec. 3.6.

3.5. Distribution of emission position

Since alpha particles are mainly emitted from the source, the top points of the alpha-particle tracks trace the shape of the radioactivity on the sample. Figures 7 (a) and 7 (b) show the anode–cathode projection distribution of the top and bottom of the alpha-particle tracks, respectively, where the top and bottom are defined as the zero and maximum drift coordinate, respectively, as shown in Fig. 5 (a) and 5 (d). The dashed line represents the edge of the drift-plate sample window. Comparing Fig. 7 (a) with Fig. 7 (b) clearly reveals the shape of the radioactivity.

The position resolution was evaluated along the four dashed lines in Fig. 7 (a). The number of events was projected onto the axis perpendicular to the lines and was fit with error functions as shown in Fig. 8. Figure 8 (a) and (b) represent the alpha-particle emission position projection to cathode and anode, respectively. The red lines are the fitting based on the error functions. As a result, the position resolution was determined to be 0.68 ± 0.14 cm (σ), where the error is a standard deviation in the four positions.

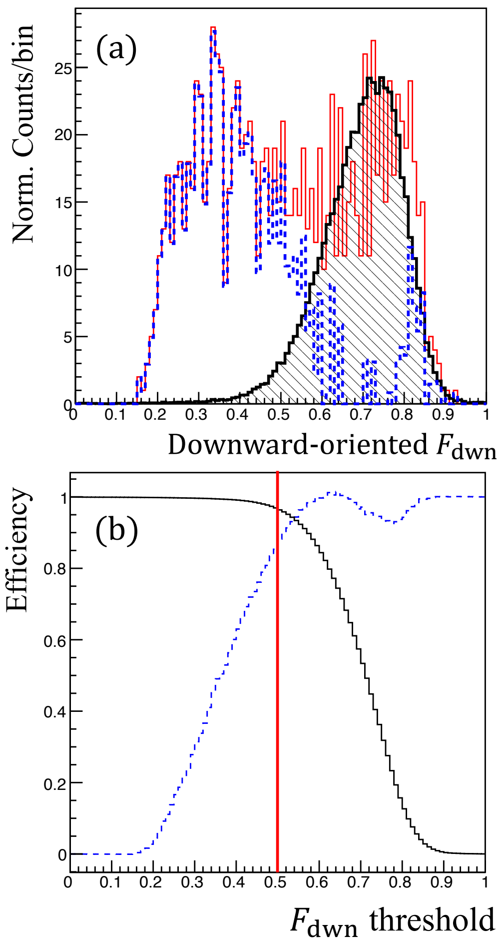

Fig. 6: (a) Downward-oriented distribution for source-α (black shade), radon-α (red solid), and a histogram made by subtracting the radon-α spectrum from the source-α one(blue dashed) (b) Detection efficiency for downward- (black solid) and rejection efficiency for upward-oriented (blue dashed) events as a function of F_{dwn} threshold.

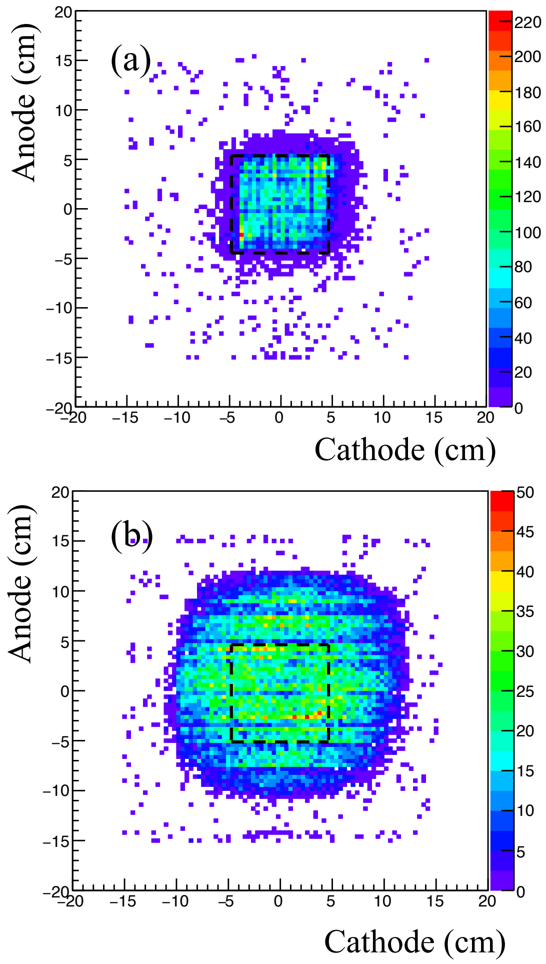

Fig. 7: Anode–cathode projection distributions of (a) top and (b) bottom of tracks for alpha particles emitted from the source. The dashed line is the edge of the sample window.

3.6. Detection and selection efficiency

To select good events for alpha particles from the sample, we use the following criteria: (C1) selection for events with good fitting tracks, (C2) cut for the upward-oriented events, and (C3) selection for events with emission points in the sample region.

For criterion C1, the best fit to track events was selected as $f_{\mathrm{min}}(\theta)/(n-1) < 0.02$ cm^2. It was determined as the best θ to minimize $f(\theta)/(n-1)$ at each plane, for both tracking of electrons and α-ray. The electron track tends to be scattered, so $f_{\mathrm{min}}(\theta)/(n-1)$ for electrons is bigger than that of α-ray. Therefore, the upper limit of $f_{\mathrm{min}}(\theta)/(n-1)$ serves to suppress electron-track events.

Criterion C2 rejects the upward-oriented tracks with > 3.5 MeV and $F_{\mathrm{dwn}} \leq 0.5$ because the determination efficiency depends on the energy. The upward- and downward-oriented tracks can be determined with 95% or more certainly at over 3.5 MeV. Note that this cut was applied for the events > 3.5 MeV, because the radon background, which was assumed to be the dominant background source, created the peak around 6 MeV and the contribution to the energy range below 3.5 MeV was limited.

For criterion C3, the source-α was selected within a region of ± 8 cm in both the anode and cathode. The cut condition was decided to cover both tails of the distribution (or $> 4\sigma$) in Fig. 8 (a) and (b). The rate of radon-α in the selected region was around two orders of magnitude lower than the source-α

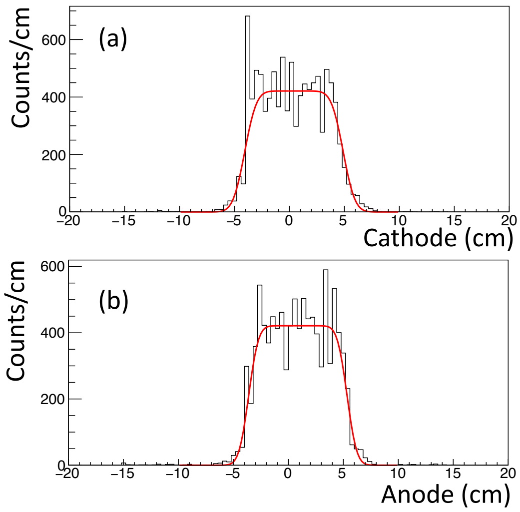

Fig. 8: Alpha-particle emission position projected to cathode (a) and anode (b). Red lines represent fitting with error functions.

rate, and considered negligible.

The selection efficiency for C1, C2, and C3 containing the detection efficiency was calculated to be $(2.17 \pm 0.29) \times 10^{-1}$ counts/α (the ratio of the count rate to the α rate of the source), where the error represents the systematic error of C1 to C3 selections and uncertainty of the source radioactivity is considered negligible.

3.7. Sample test and background estimate

3.7.1. Setup

A 5 cm $\times$ 5 cm piece of the standard μ-PIC whose α rate was known to be 0.28 ± 0.12 $\alpha/\mathrm{cm}^2/\mathrm{hr}$ in previous work [16] served as a sample and was inspected by using the detector. A photograph of the sample position over the setup mesh is shown in Fig. 9. The measurement live time was 75.85 hr.

3.7.2. Background in sample region

The α rate of the sample was estimated by subtracting the background rate. Considered background was mainly the radon-α. The detector measured both the α rates in the region of the sample and around the sample (outer region). The background rate could be determined from the α rate in the outer region. Recall, the upward and downward radon-α rates are same. The sample-α has mainly downward-oriented. Thus, the background rate could be estimated by the upward rate in the sample region and independently cross-checked by the upward rate in the outer region.

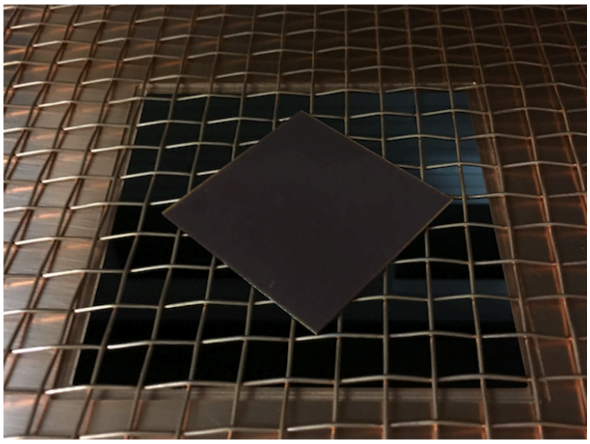

Fig. 9: Setup for a 5 cm $\times$ 5 cm piece of the standard μ-PIC as sample.

We checked the upward-oriented ($F_{\mathrm{dwn}} \leq 0.5$) α rate in both regions because the alpha particles from a sample are typically emitted downward. Measured energy spectra are shown in Fig. 10. The red- and black-shaded histograms show the energy spectra inside and outside the sample region, respectively. These spectra are scaled by the selection efficiency. Both peaks are around 6 MeV and α rates are $(2.16^{+0.54}_{-0.35}) \times 10^{-2}$ (inside) and $(1.54^{+0.64}_{-0.40}) \times 10^{-2}$ $\alpha/\mathrm{cm}^2/\mathrm{hr}$ (outside). Therefore, the background condition inside the sample region is compatible at less than 1σ with the background condition outside the sample region. The alpha-particle energy spectrum is interpreted as the radon peaks at 5.5 MeV (^{222}Rn), 6.0 MeV (^{218}Po), and 7.7 MeV (^{214}Po).

The downward-oriented ($F_{\mathrm{dwn}} > 0.5$) α rate outside the sample is $(1.58^{+0.29}_{-0.26}) \times 10^{-2}$ $\alpha/\mathrm{cm}^2/\mathrm{hr}$, as shown in the black-shaded spectrum of Fig. 11. In this work, the background rate was improved by one order of magnitude in comparison with that of our previous work [16]. The background reduction is attributed to the track-sense determination to reject upward-oriented alpha (for > 3.5 MeV) and the replacement of the low-α μ-PIC (for ≤ 3.5 MeV). In the energy region between 2.0 and 4.0 MeV, where most radon background is suppressed, the background rate is $(9.6^{+7.9}_{-5.6})\times 10^{-4}$ $\alpha/\mathrm{cm}^2/\mathrm{hr}$.

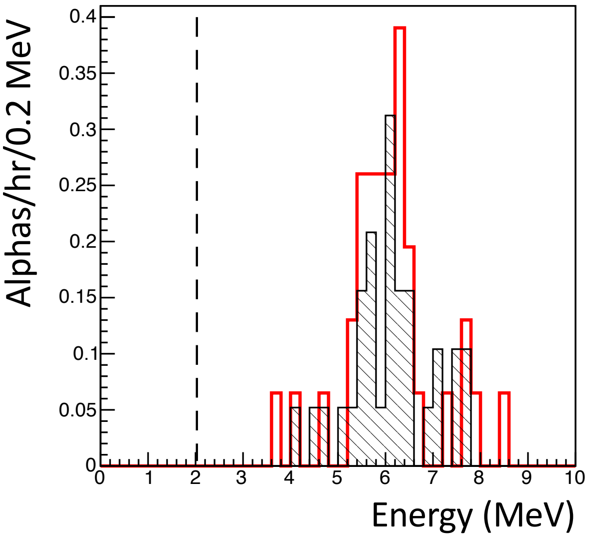

Fig. 10: Upward-oriented alpha-particle energy spectra inside (red) and outside (black shade) the sample region. The dashed line is the threshold of 2 MeV.

3.7.3. α rate of sample

Figure 12 shows the distribution of the top of the tracks for the sample, where the candidates are selected by the criteria C1 and C2. The regions ① and ② are defined as sample and background regions, respectively. The sample region corresponds to the sample window. The sample region is the inside of ± 5 cm of anode and cathode. The background region is the outside of the sample region and the inside of ± 7.5 cm of anode and cathode. The systematic uncertainty due to the setting of the background region is estimated by changing the outer bound by $\pm$ 0.5cm to be $\sim$ 0.5%. Figure 11 shows the energy spectra of downward-oriented alpha particles in the sample (red) and the background region (black shaded). The α rate of the sample was calculated to be $(3.57^{+0.35}_{-0.33}) \times 10^{-1}$ $\alpha/\mathrm{cm}^2/\mathrm{hr}$ (> 2.0 MeV) by subtracting the background rate.

Here, the impurity of ^{232}Th and ^{238}U is estimated by comparing with a prediction of α rate spectrum in the simulation, where it mentions that the isotope in the material is assumed as only ^{232}Th or ^{238}U because of the continuous α rate spectrum. In the fit region between 2 and 10 MeV, the impurity of ^{232}Th or ^{238}U is estimated to be 6.0 ± 1.4 or 3.0 ± 0.7 ppm, respectively. The impurities of ^{232}Th and ^{238}U are measured to be 5.84 ± 0.03 and 2.31 ± 0.02 ppm, respectively, by using the HPGe detector with the measuring time of 308 hr. Although the error is huge because of the continuous energy spectrum, it is consistent with the prediction of prior measurement. In this sample test, it was demonstrated to observe the background alphas at the same time.

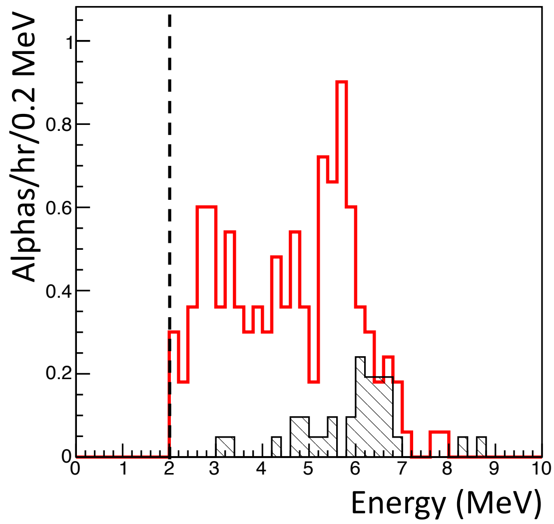

Fig. 11: Downward-oriented alpha-particle energy spectra in sample region (red) and background region (black shade). The dashed line is the threshold of 2 MeV.

4. Discussion

We begin by discussing the sensitivity for the energy between 2 and 9 MeV based on long-term measurements. In this energy range, the background is dominated by the radon-α's with $\sim (1.58^{+0.29}_{-0.26}) \times 10^{-2}$ $\alpha/\mathrm{cm}^2/\mathrm{hr}$. The statistical error (σ) is expected to scale with the inverse of the square root of the measurement time (t) given as $\sigma \propto 1/\sqrt{t}$. In this work, the live time was only three days, and the statistical error was $\sigma \sim 3 \times 10^{-3} \alpha/\mathrm{cm}^2/\mathrm{hr}$. With a measurement time of one month, the error of sample-α's was estimated to be $\sigma \sim 1 \times 10^{-3}$ $\alpha/\mathrm{cm}^2/\mathrm{hr}$. The sensitivity for a sample with a radioactivity much lower than the background rate is practically determined by the statistics of the background when the background can be subtracted. The expected statistical errors of both the background and sample are 1×10^{-3} $\alpha/\mathrm{cm}^2/\mathrm{hr}$ with one month of measurement time. The statistical error of the subtracted event rate, or the detection sensitivity of the sample, is therefore expected to be a few $\times 10^{-3}$ $\alpha/\mathrm{cm}^2/\mathrm{hr}$.

	This work	HPGe detector
Sample volume (cm)	$(5 \times 5) \times 0.098$	$(5 \times 5) \times 2.47$
Sample weight (g)	6.8	169.5
Measureing time (hr)	75.85	308
Net α rate (α/cm^2/hr))	$(3.57^{+0.35}_{-0.33}) \times 10^{-1}$	—
^{232}Th impurities (ppm)	6.0 ± 1.4	5.84 ± 0.03
^{238}U impurities (ppm)	3.0 ± 0.7	2.31 ± 0.02

Table 1: Comparison of Screening result with this work and HPGe detector.

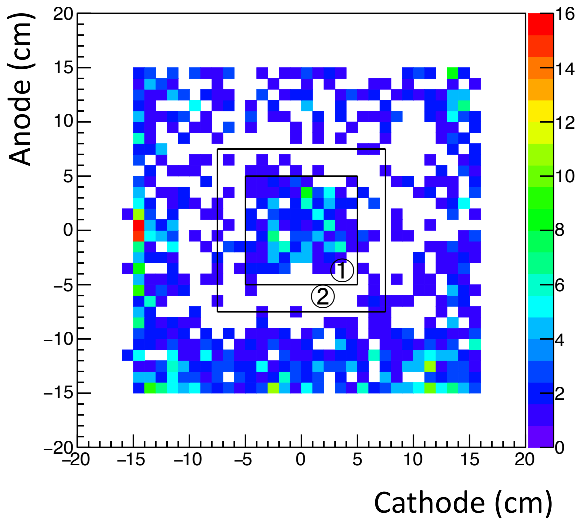

Fig. 12: Distribution of the top of downward-oriented alpha-particle track. The regions ① and ② are the sample and background regions, respectively.

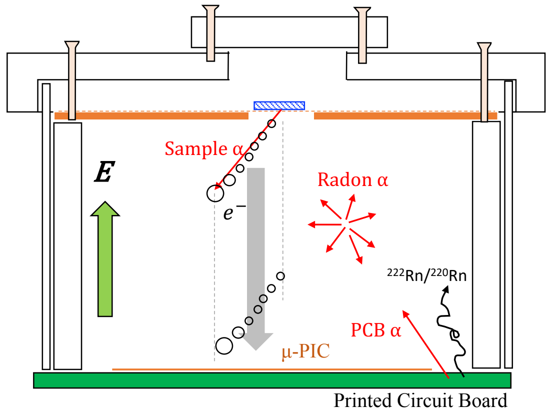

Fig. 13: Schematic cross section of background alpha particles in detector setup.

The edges region (anode $\sim \pm 15$ cm or cathode $\sim \pm 15$ cm) has a high rate of background, as shown in Fig. 12. These events have an energy and path-length dependence similar to that of the alpha particles. The alpha particles were mainly oriented upward and were emitted from outside the detection area, limited by the μ-PIC. As an impurity candidate, a piece of the printed circuit board (PCB) was inspected and the α rate was $(1.16 \pm 0.06) \times 10^{-1}$ α/cm^2/hr. Although the alpha-particle events could be rejected by the fiducial region cut, these impurities could be the radon sources (see Fig. 13). Therefore, as a next improvement, a material with less radiative impurities should be used for the PCB.

The goal for detector sensitivity is less than 10^{-4} α/cm^2/hr. We can potentially reduce the background rate by using the cooled charcoal to suppress radon gas and using a material with less impurities. Insulators such as polytetrafluoroethylene, polyimide, and polyetheretherketone, are in general low radioactive if we can use them without extra materials with relatively high radioactive like reinforcing glass-cloth. A recent study reported that a cooled charcoal could suppress the radon by 99% in the argon gas [20]. A recent NEWAGE detector suppresses the radon to 1/50 by using cooled charcoal [5]. With these improvements, the detector would achieve to the goal of performance.

5. Conclusion

We developed a new alpha-particle imaging detector based on the gaseous micro-TPC. The measured energy resolution is 6.7% (σ) for 5.3 MeV alpha particles. The measured position resolution is 0.68 ± 0.14 cm. Based on a waveform analysis, the downward-oriented events' selection efficiency is 0.964 ± 0.004 and the cut efficiency of the upward-oriented events is 0.85 ± 0.04 at > 3.5 MeV. Also, a piece of the standard μ-PIC was measured as a sample, and the result is consistent with the one obtained by a measurement done with a HPGe detector. A measurement of the alpha particles from a sample and background was also established at the same time. A background rate near the radon-α ($(1.58^{+0.51}_{-0.42}) \times 10^{-2}$ α/cm^2/hr) was achieved.

Acknowledgments

This work was supported by a Grant-in-Aid for Scientific Research on Innovative Areas, 26104004 and 26104008, from the Japan Society for the Promotion of Science in Japan. This work was supported by the joint research program of the Institute for Cosmic Ray Research (ICRR), the University of Tokyo. We thank Dr. Y. Nakano of the ICRR, University of Tokyo, Japan for providing us with a helium-gas leak detector.

References

[1] R Bernabei, et al., J. Phys. Conf. Ser. **1056** (2018) 012005.

[2] XENON Collaboration, Eur. Phys. J. **77** 881 (2017).

[3] D. S. Akerib, et al., Phys. Rev. Lett. **118** 021303 (2017).

[4] T. Tanimori, et al., Phys. Lett. B **578** (2004) 241.

[5] K. Nakamura, et al., Prog. Theo. Exp. Phys. (2015) 043F01.

[6] The GERDA Collaboration, Nature **544** (2017) 47.

[7] A. Gando, et al., Phys. Rev. Lett. **117** 082503 (2016).

[8] D. S. Leonard, et al., Nucl. Instr. Meth. A **871** (2017) 169.

[9] N. Abgrall, et al., Nucl. Instr. Meth. A **828** (2016) 22.

[10] R. Arnold, et al., Eur. Phys. J. C **78** (2018) 821.

[11] R. Arnold, et al., PRL **119**, 041801 (2017).

[12] A. S. Barabash, et al., JINST **12** (2017) P06002.

[13] K. Abe, et al., Nucl. Instr. Meth. A **884** (2018) 157.

[14] K. Miuchi, et al., Phys. Lett. B **686** (2010).

[15] K. Miuchi, et al., Phys. Lett. B **654** (2007) 58.

[16] T. Hashimoto, et al., AIP Conf. Proc. **1921**, 070001 (2018).

[17] T. Hashimoto, et al., in preparation.

[18] R. Orito, et al., IEEE Trans. Nucl. Scie. **51**, 4 (2004) 1337.

[19] H. Kubo, et al., Nucl. Instr. Meth. A **513** (2003) 93.

[20] M. Ikeda, et al., Radioisotopes, **59**, (2010) 29.

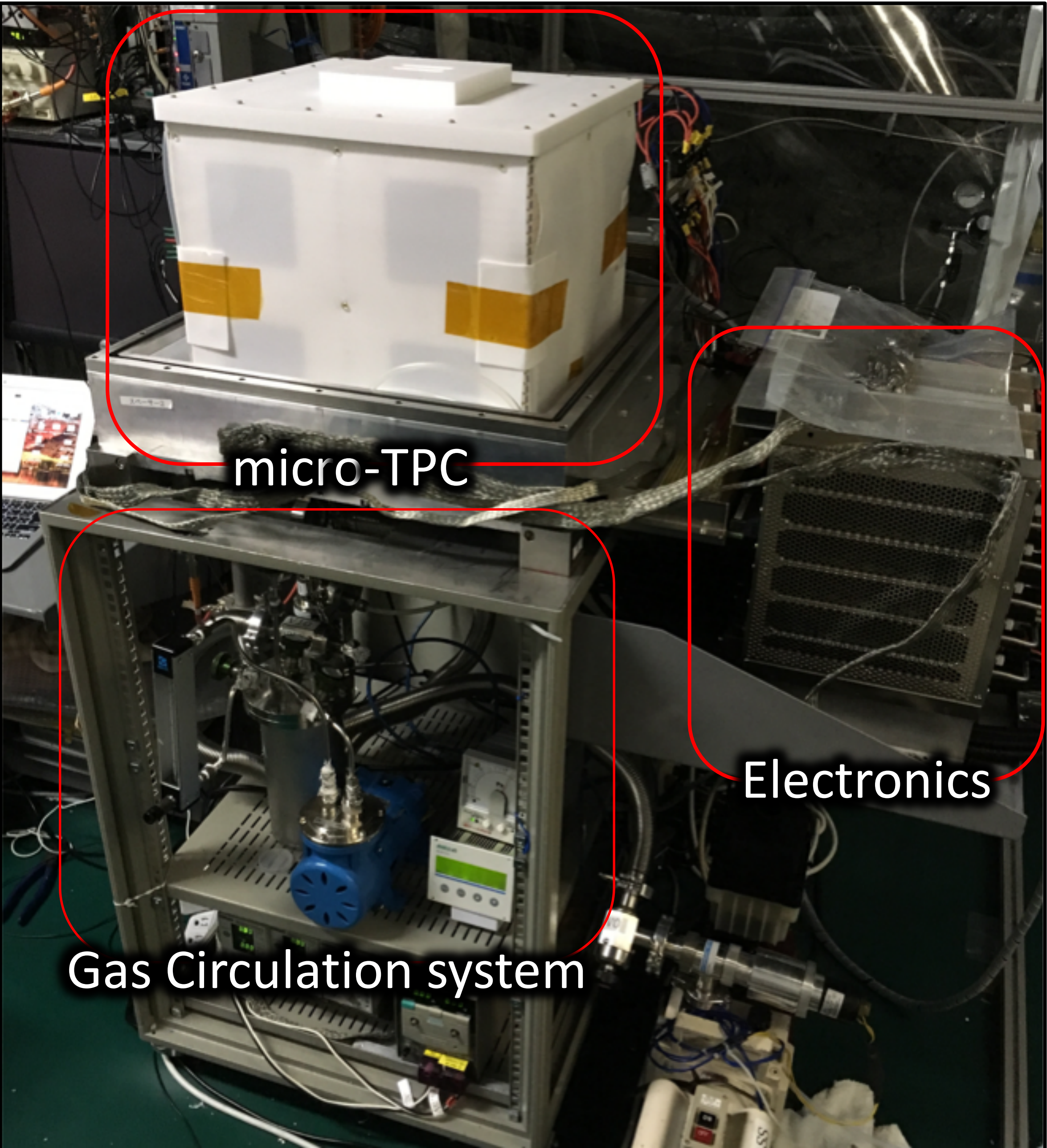
micro-TPC
Electronics
Gas Circulation system

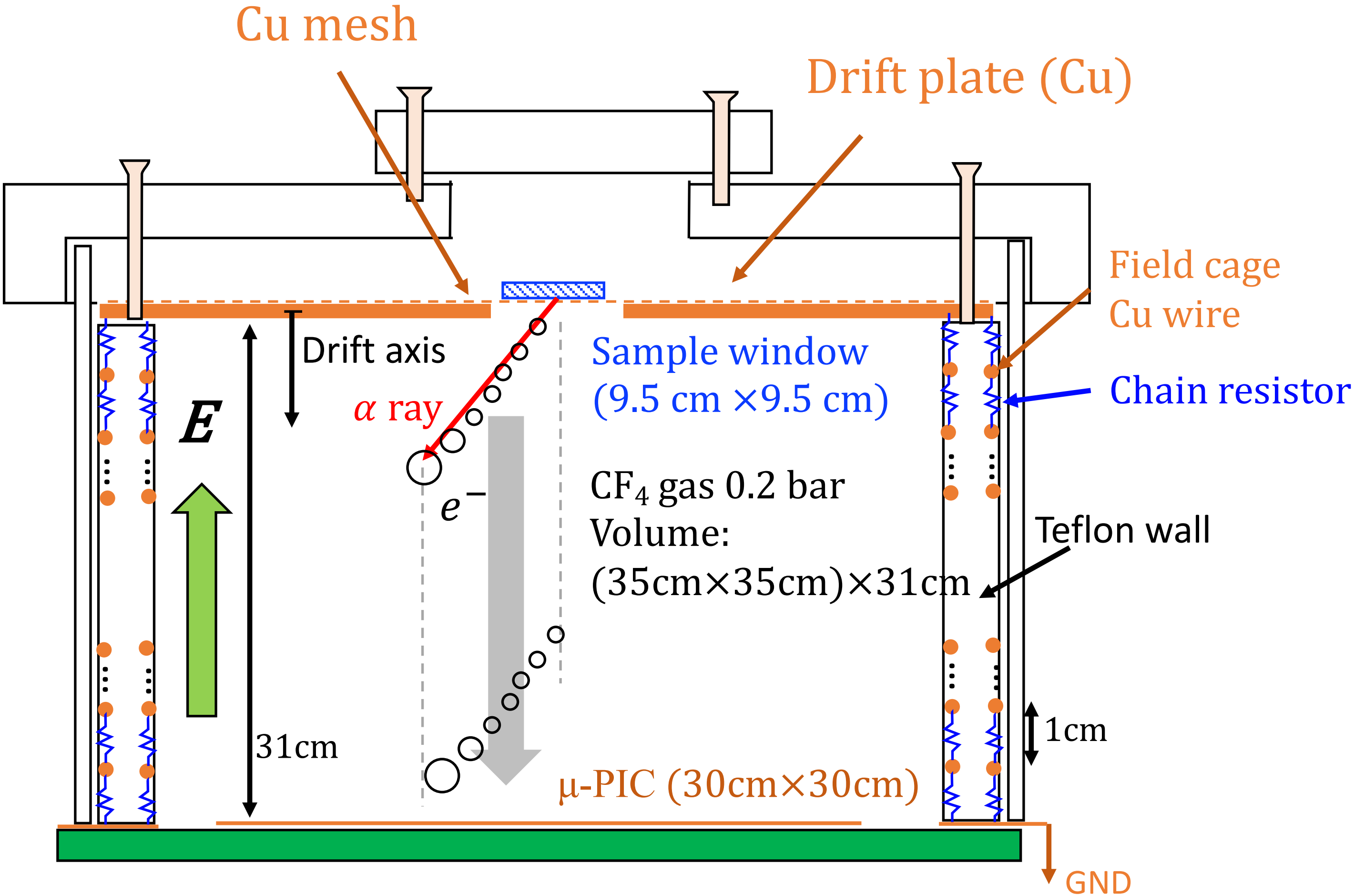

Cu mesh
Drift plate (Cu)
Field cage
Cu wire
Sample window
(9.5 cm ×9.5 cm)
Chain resistor
Drift axis
α ray
E
e−
CF4 gas 0.2 bar
Volume:
(35cm×35cm)×31cm
Teflon wall
1cm
31cm
μ-PIC (30cm×30cm)
GND

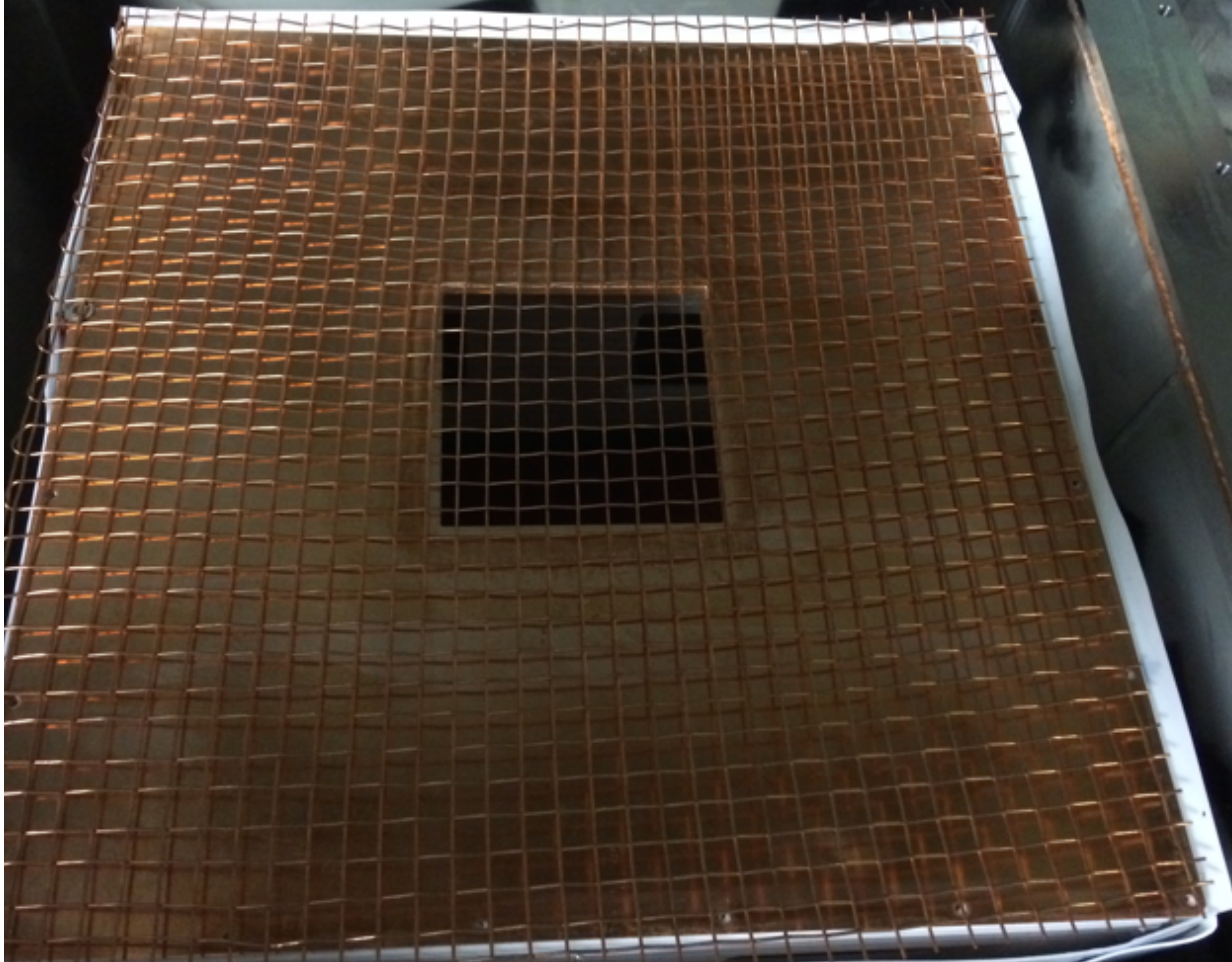

gure4

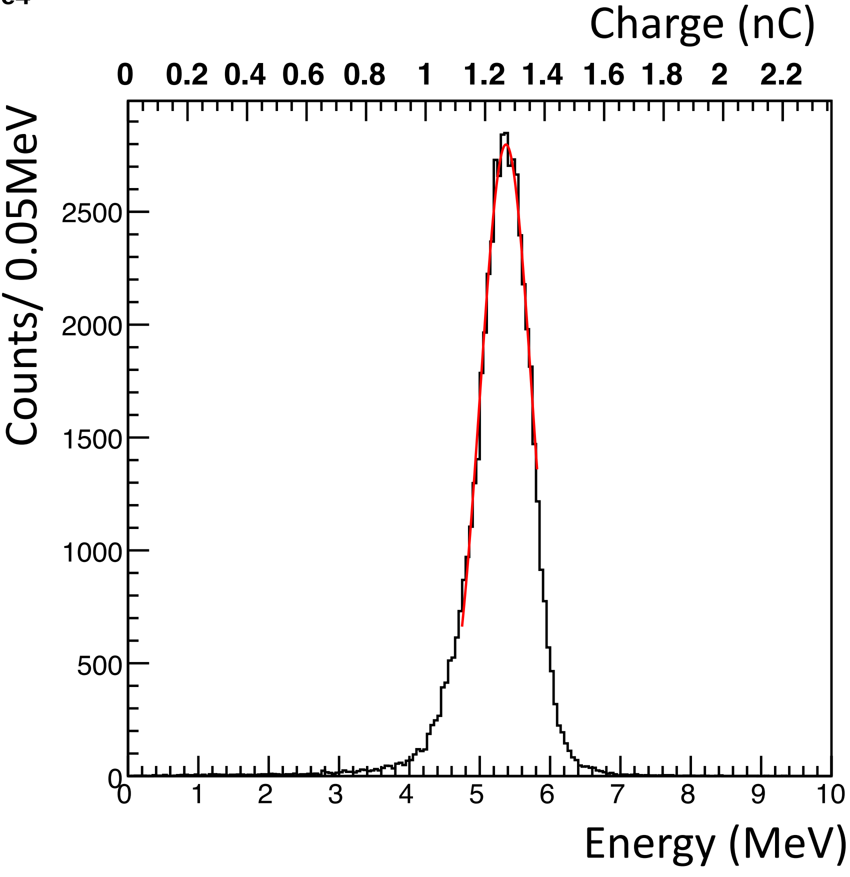

Charge (nC)
0
0.2
0.4
0.6
0.8
1
1.2
1.4
1.6
1.8
2
2.2
Counts/ 0.05MeV
2500
2000
1500
1000
500
0
0
1
2
3
4
5
6
7
8
9
10
Energy (MeV)

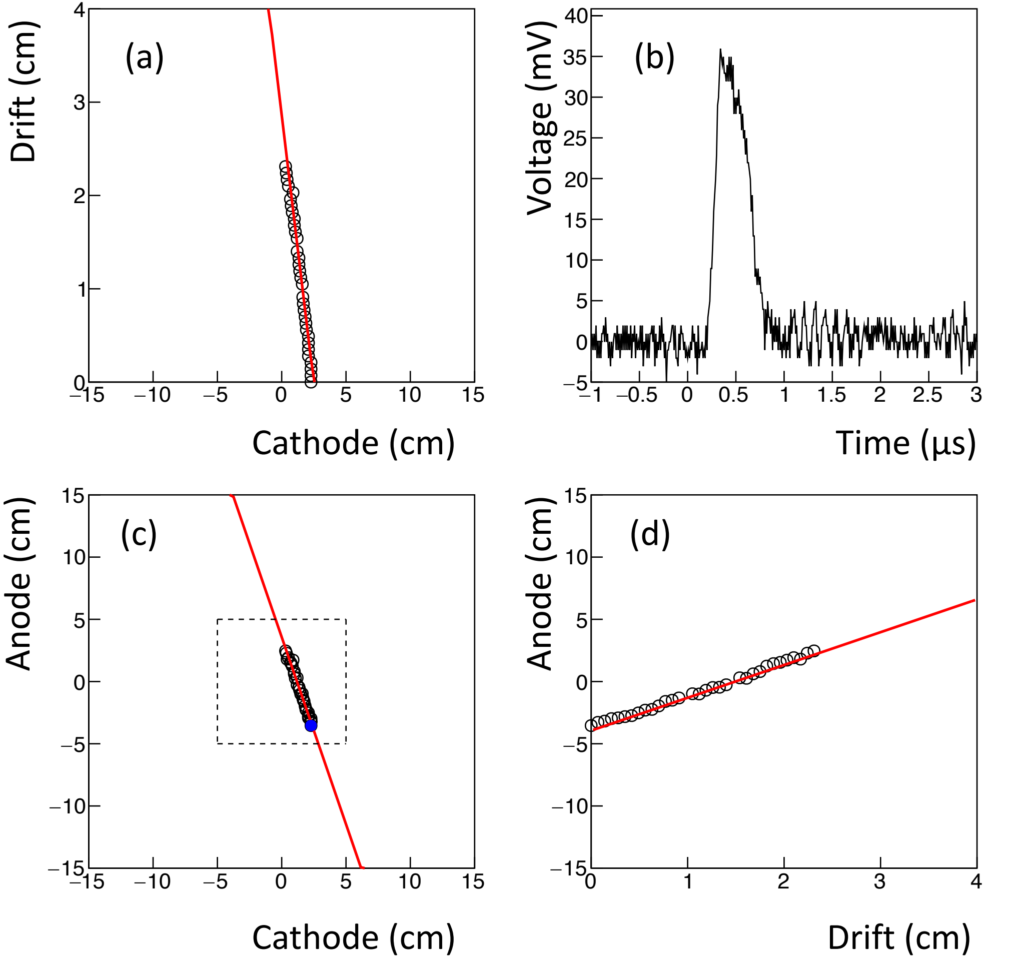
(a)
Drift (cm)
Cathode (cm)
(b)
Voltage (mV)
Time (μs)
(c)
Anode (cm)
Cathode (cm)
(d)
Anode (cm)
Drift (cm)

gure6

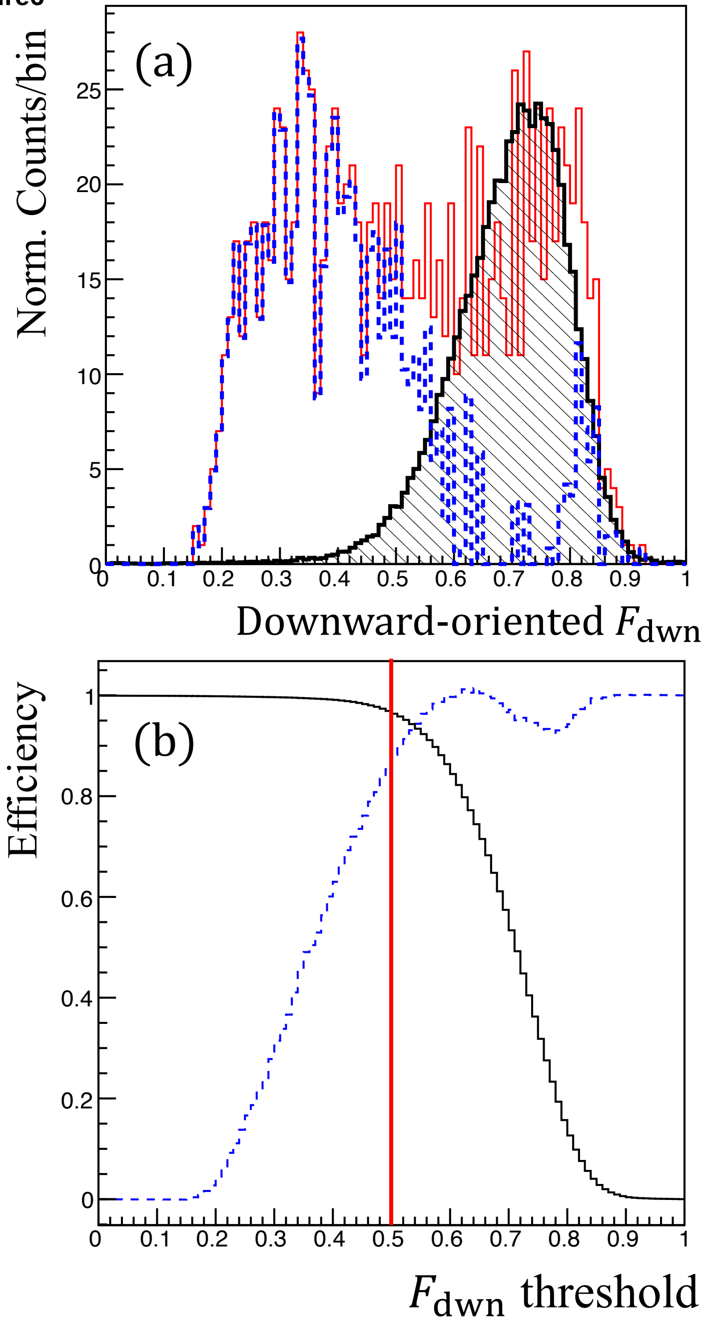
(a)
Norm. Counts/bin
25
20
15
10
5
0
0
0.1
0.2
0.3
0.4
0.5
0.6
0.7
0.8
0.9
1
Downward-oriented F_{dwn}
(b)
Efficiency
1
0.8
0.6
0.4
0.2
0
0
0.1
0.2
0.3
0.4
0.5
0.6
0.7
0.8
0.9
1
F_{dwn} threshold

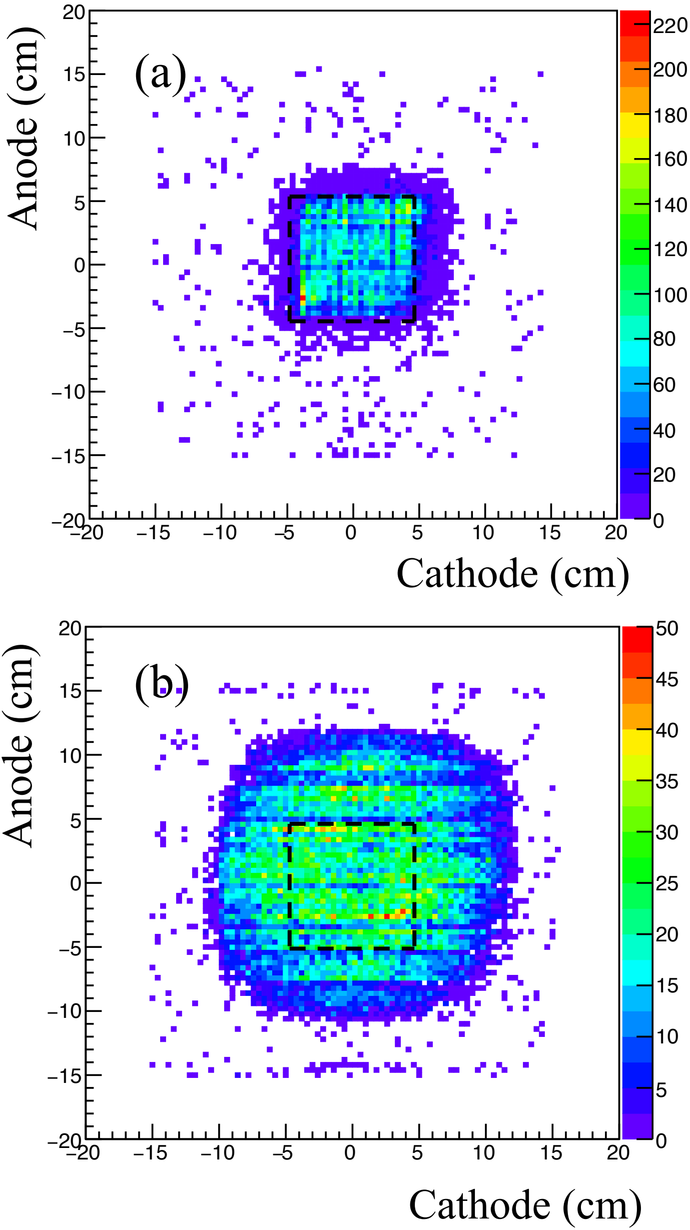

(a)
Anode (cm)
Cathode (cm)
20
15
10
5
0
−5
−10
−15
−20
220
200
180
160
140
120
100
80
60
40
20
0
(b)
Anode (cm)
Cathode (cm)
50
45
40
35
30
25
20
15
10
5
0

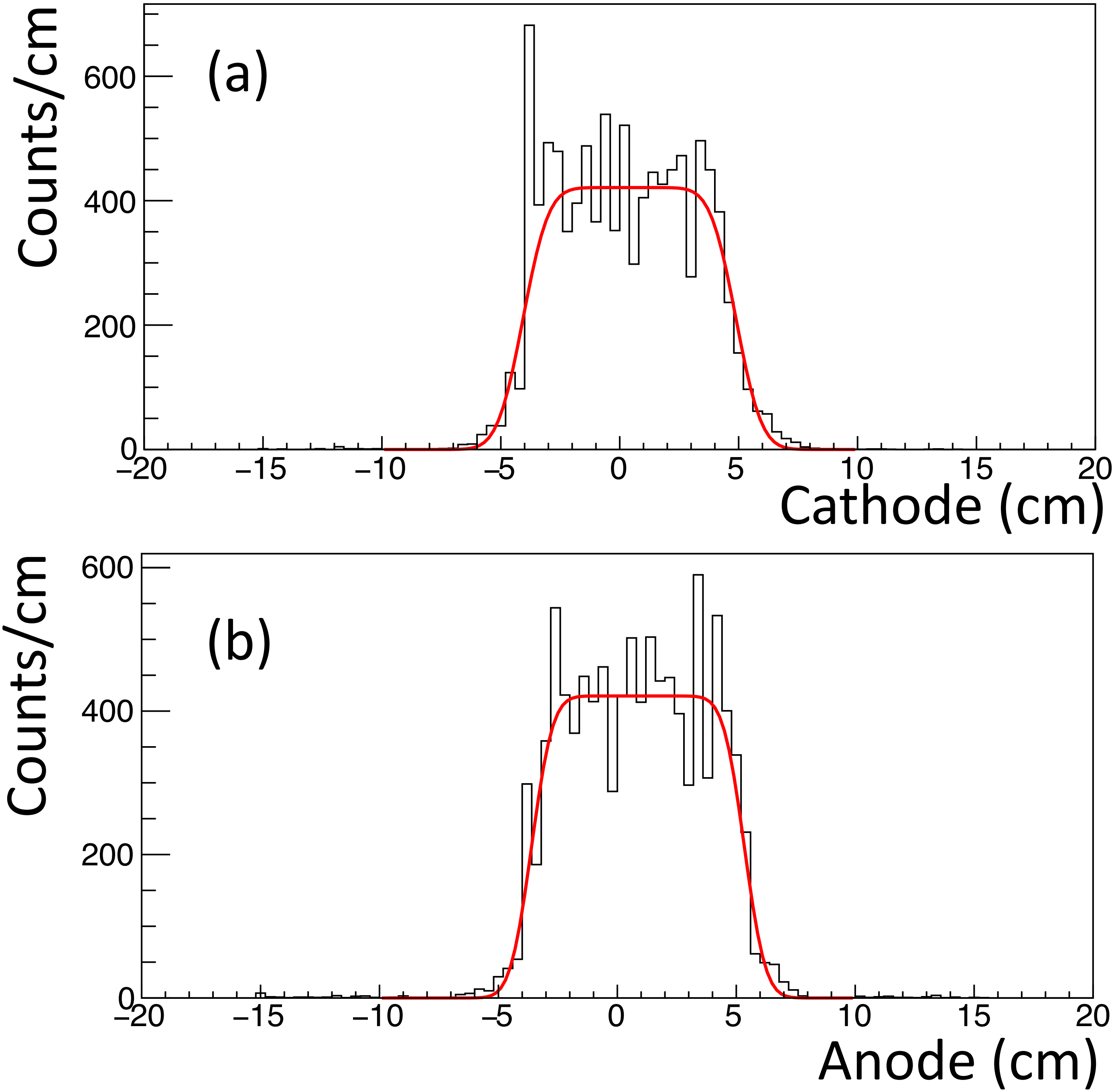

(a)
Counts/cm
0
200
400
600
−20
−15
−10
−5
0
5
10
15
20
Cathode (cm)
(b)
Counts/cm
0
200
400
600
−20
−15
−10
−5
0
5
10
15
20
Anode (cm)

Figure9

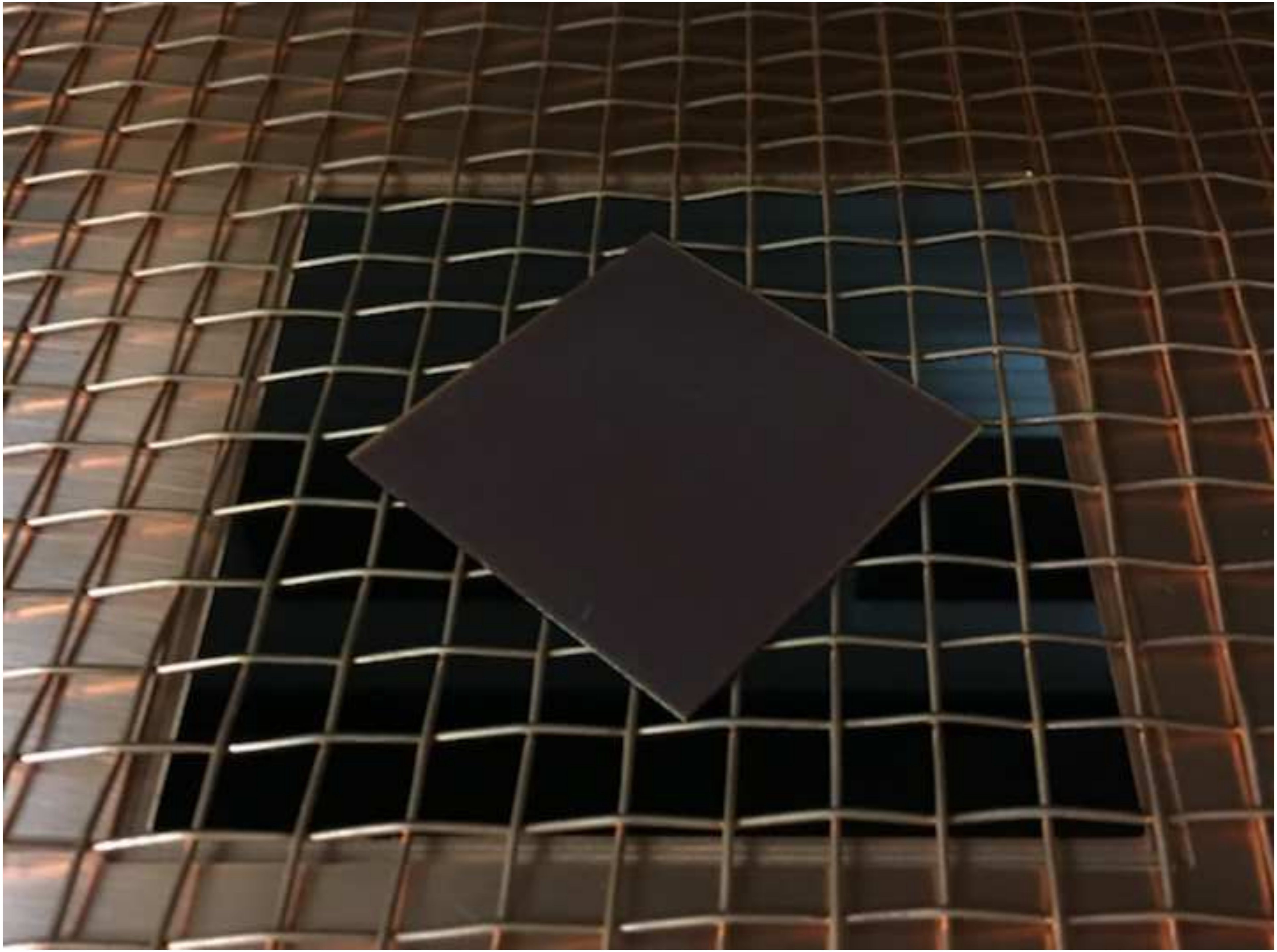

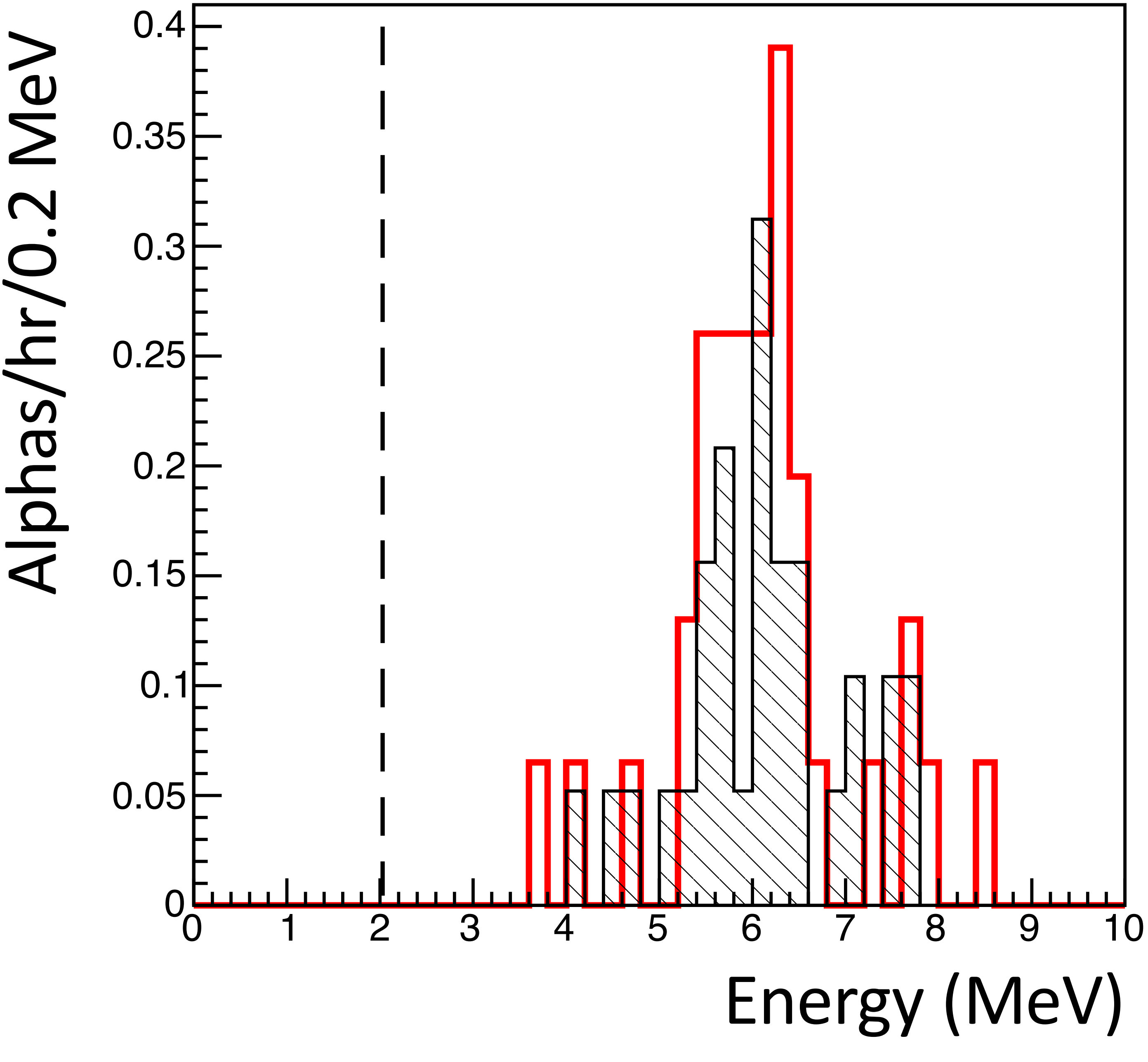

Alphas/hr/0.2 MeV
0.4
0.35
0.3
0.25
0.2
0.15
0.1
0.05
0
0
1
2
3
4
5
6
7
8
9
10
Energy (MeV)

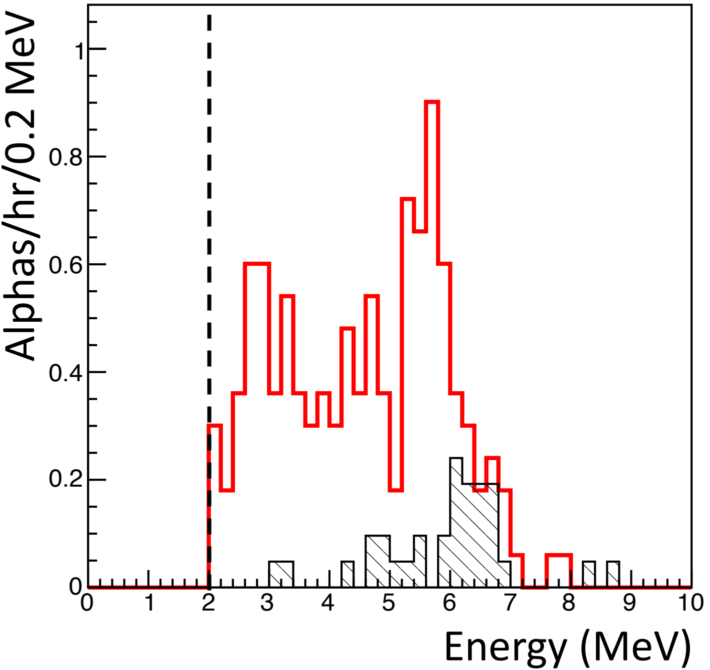

Alphas/hr/0.2 MeV
0
0.2
0.4
0.6
0.8
1
0
1
2
3
4
5
6
7
8
9
10
Energy (MeV)

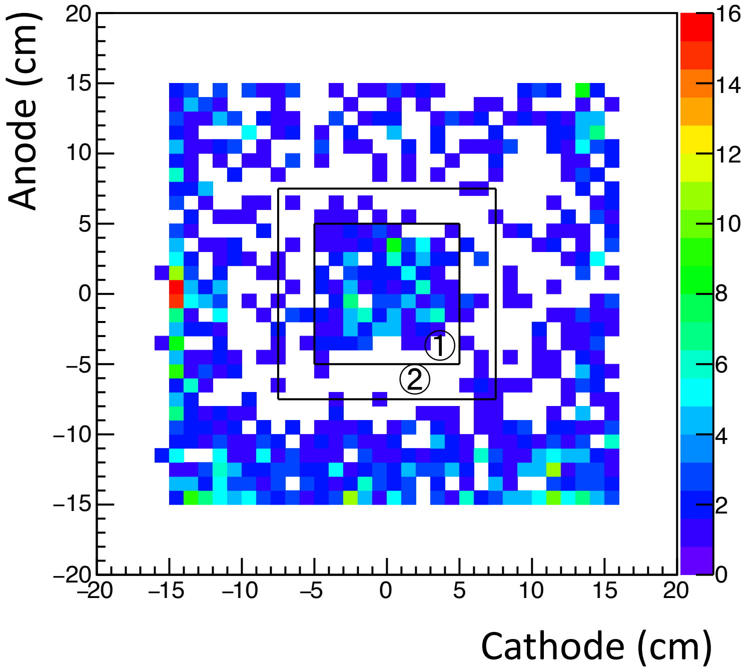

Anode (cm)
Cathode (cm)
20
15
10
5
0
−5
−10
−15
−20
1
2
16
14
12
10
8
6
4
2
0

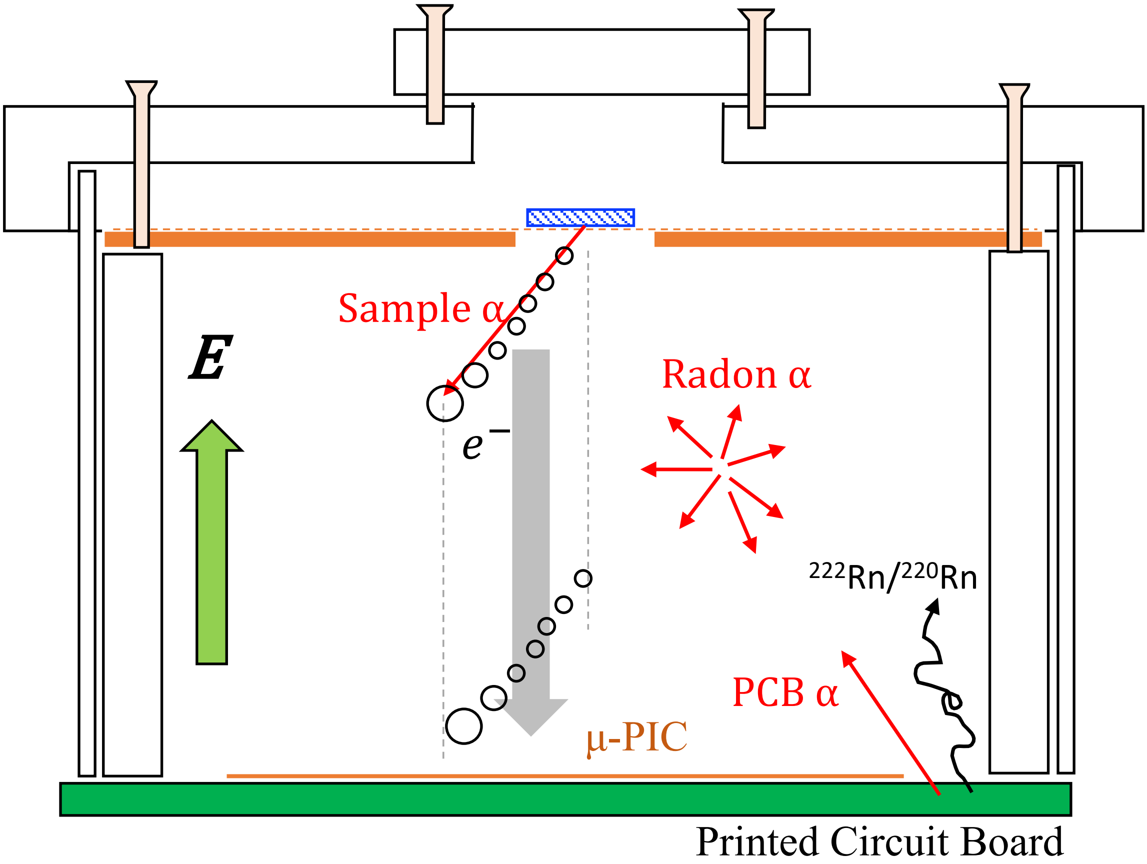
Sample α
E
Radon α
e⁻
²²²Rn/²²⁰Rn
PCB α
μ-PIC
Printed Circuit Board

	This work	HPGe detector
Sample volume (cm)	$(5 \times 5) \times 0.098$	$(5 \times 5) \times 2.47$
Sample weight (g)	6.8	169.5
Measureing time (hr)	75.85	308
Net α rate (α/cm^2/hr))	$(3.57^{+0.35}_{-0.33}) \times 10^{-1}$	—
^{232}Th impurities (ppm)	6.0 ± 1.4	5.84 ± 0.03
^{238}U impurities (ppm)	3.0 ± 0.7	2.31 ± 0.02

Table 1: Comparison of Screening result with this work and HPGe detector.

Dear reviewer #1,

Thank you for your advices.

Dear Reviewer #2,

Thank you for your advices. I think our paper has been improved clearly due to your suggestions. The replies for your comments and questions are follows. And you can see revised manuscript and difference one. The corrected sentences have been indicated as a red with remove-line (old) and blue (new) one.

Suggest title would read better by changing "radioactive" to "radioactivity"

>> Title was revised as “Development of alpha-particle imaging detector based on a low radioactivity micro-time-projection chamber”.

Line 5-6: change to "...searching for dark matter, arguably a direct detection has not been observed".

>> It was revised at line 5-6.

Line 181: Change "flush" to "flash".

>> It was revised at line 181.

Line 186: replace "worse than" with "not as good as".

>> It was revised at line 186.

Line 239-240: I agree that it makes sense that half of the events can be rejected due to the upward cut. But have you some data to prove such an assumption? I worry that there are some detector orientation or design issues that may make assumption invalid. The remainder of this section relies heavily on the assumption.
>> In Sec. 3.7.2, a result of radon-alpha rates of the upward and downward in region ② is shown. The data are shown in lines 375 and 383, and histograms in Fig.10 and 11.

- Upward oriented alpha rate: $1.54^{+0.64}_{-0.40} \times 10^{-2}\ \alpha/\mathrm{cm}^2/\mathrm{h}$
- Downward oriented alpha rate: $1.58^{+0.29}_{-0.29} \times 10^{-2}\ \alpha/\mathrm{cm}^2/\mathrm{h}$

These results are consistent within the statistical errors and thus the assumption of upward and downward symmetry is shown.

Line 312: replace "good" with "best".
>> It was revised at line 312 .

Line 313: Replace "is" with "was".
>> It was revised at line 313.

Line 315: change to "...tracking of electrons...".
>> It was revised at line 315.

Line 317: change to "...for electrons..."
>> It was revised at line 317.

Line 319: change to "...serves to suppress...".
>> It was revised at line 319.

Line 334: (or >4...
>> It was revised at line 334.

Line 337: change to "and considered negligible".
>> It was revised at line 337.

Line 360: change to "Recall, the upward and down..."
>> It was revised at line 360.

Line 441–447: It's not clear what you are trying to say here. Are you saying that when the standard deviation of the sample counts matched that observed for the radon that is what dictated the sample time?

>> We apology for the misleading sentence. So, the sentence was revised to

> The sensitivity for a sample with a radioactivity much lower than the background rate is practically determined by the statistics of the background when the background can be subtracted. The expected statistical errors of both the background and sample are 1×10^{-3} $\alpha/cm^2/hr$ with one month of measurement time. The statistical error of the subtracted event rate, or the detection sensitivity of the sample, is therefore expected to be a few $\times10^{-3}$ $\alpha/cm^2/hr$.

at line 441–451.

Line 470–472: Commercial copper with lower impurities than ppb levels of U and Th is readily available and may be better than the suggested materials.

>> We apology for the misleading sentence. We meant to replace mu-PIC and PCB (not copper) with clean materials. Previous sentence means about copper plate for sample material. We consider this sentence about "copper estimate" is explained in detail but might make to mislead for readers. So that, it was simply and clearly revised to

(revised) The goal for detector sensitivity is less than 10^{-4} $\alpha/cm^2/hr$. We can potentially reduce the background rate by using the cooled charcoal to suppress radon gas and using a material with less impurities. Insulators such as polytetrafluoroethylene, polyimide, and polyetheretherketone, are in general low radioactive if we can use them without extra materials with relatively high radioactive like reinforcing glass-cloth.

(original) The goal for detector sensitivity is less than 10^{-4} $\alpha/cm^2/hr$, which corresponds to measuring radioactive impurities at the ppb level. Here, this level was estimated as an assumption of ^{238}U or ^{232}Th in 1-mm-thick copper plate. We can potentially improve the background rate by using the cooled charcoal to suppress radon gas and using a material with less impurities such as polytetrafluoroethylene, polyimide, and polyetheretherketone without glass fibers.

at line 467–475.

A difference with revised one

Development of an alpha-particle imaging detector based on a low radioactiveradioactivity micro-time-projection chamber

H. Ito[a*], T. Hashimoto[a], K. Miuchi[a], K. Kobayashi[b,c], Y. Takeuchi[a,c], K. D. Nakamura[a], T. Ikeda[a], and H. Ishiura[a]

[a] *Kobe University, Kobe, Hyogo 657-8501, Japan.*

[b] *Institute for Cosmic Ray Research (ICRR), the University of Tokyo, Kashiwa, Chiba 277-8582 Japan.*

[c] *Kavli Institute for the Physics and Mathematics of the Universe (WPI), The University of Tokyo Institutes for Advanced Study, University of Tokyo, Kashiwa, Chiba 277-8583, Japan.*

Abstract

An important issue for rare-event-search experiments, such as the search for dark matter or neutrinoless double beta decay, is to reduce radioactivity of the detector materials and the experimental environment. The selection of materials with low radioactive impurities, such as isotopes of the uranium and thorium chains, requires a precise measurement of surface and bulk radioactivity. Focused on the first one, an alpha-particle detector has been developed based on a gaseous micro-time-projection chamber. A low-α μ-PIC with reduced alpha-emission background was installed in the detector. The detector offers the advantage of position sensitivity, which allows the alpha-particle contamination of the sample to be imaged and the background to be measured at the same time. The detector performance was measured by using an alpha-particle source. The measurement with a sample was also demonstrated and the sensitivity is discussed.

Keywords: Alpha-particle detector, Position sensitivity, Time projection chamber, μ-PIC, Low background

1. Introduction

Approximately 27% of the universe is dominated by non-baryonic matter, called dark matter. Although many experimental groups have been ~~searching for dark matter, any direct detection has yet been detected.~~ searching for dark matter, arguably a direct detection has not been observed. Typical experiments that search for dark matter are performed by using massive, low-background detectors. Although the DAMA group has observed the presumed annual modulation of dark matter particles in the galactic halo with a significance of 9.3σ [1], other groups such as XENON1T [2] and LUX [3] were unable to confirm these results. Meanwhile, a direction-sensitive method has been focused because of an expected clear anisotropic signal due to the motion of the solar system in the galaxy [4]. The NEWAGE group precedes a three-dimensionally sensitive dark matter search with a micro-time-projection chamber (micro-TPC), being the main background surface alpha particles from ^{238}U and ^{232}Th in the detector materials or in the μ-PIC [5].

Neutrinoless double beta ($0\nu\beta\beta$) decay is a lepton-number-violating process, which suggests the neutrino as a Majorana particle (i.e. it is its own antiparticle). Experiments like GERDA [6] and KamLAND-Zen [7] have been able to set a lower limit on the half-life over 10^{25} yr and 10^{26} yr at 90%CL by using ^{76}Ge and ^{136}Xe, respectively, but no positive signal of the $0\nu\beta\beta$ process has been observed yet. Conversely, a tracking system for two electrons provides strong evidence of the $0\nu\beta\beta$ decay process. The $0\nu\beta\beta$ background has been well investigated as radioactive impurities such as ^{238}U and ^{232}Th decay-chain isotopes, ^{40}K, ^{60}Co, ^{137}Cs including in the de-

*Corresponding author. E-mail address: ito.hiroshi@crystal.kobe-u.ac.jp (H. Ito).

tector material, which emit γ with around MeV [8, 9]. The NEMO3 group set lower limits at $T_{1/2}(0\nu\beta\beta) > 2.5 \times 10^{23}$ yr (90%CL) for ^{82}Se [10], and $T_{1/2}(0\nu\beta\beta) > (1.1 - 3.2) \times 10^{21}$ yr (90%CL) for ^{150}Nd [11]. For this experiment background is dominated by the ^{208}Tl and ^{214}Bi contamination present in the double beta emitter source foils. The SuperNEMO group has developed the BiPo-3 detector to measure the radioactive impurities in these foils with a sensitivity less than 2 μBq/kg (90%CL) for ^{208}Tl and 140 μBq/kg (90%CL) for ^{214}Bi [12]. Therefore, the background of $0\nu\beta\beta$ decay is not only a contamination by the end point of continuous energy in an ordinary $2\nu\beta\beta$ decay process, but also the radiative impurities such as ^{238}U and ^{232}Th in the detector.

To estimate the radioactive impurities in the detector materials, the XMASS group measured ^{210}Pb and ^{210}Po in the bulk of copper by using a commercial alpha-particle detector (Ultra-Lo 1800, XIA) [13]. The alpha detector has a good energy resolution (as explained in Sec. 3.2) and a mechanism to reduce the background by waveform analysis, and thus its sensitivity is $\sim 10^{-4}$ α/cm^2/hr. However, it has no position sensitivity. A sample such as a micro pattern gas detector board does not have a uniform radioactive contamination. For example the impurities can be in a particular location due to the manufacturing process. Therefore, a position-sensitive alpha detector is required in order to determine the site and perhaps the process associated with the materials contamination.

This paper is organized as follows. The details of the alpha-particle detector, setup, low-α micro pixel chamber (μ-PIC), gas circulation system, electronics, and trigger and data acquisition systems are described in Sec. 2. The performance check that uses the alpha-particle source, a sample test, and background estimation are described in Sec. 3. The remaining background of the detector and future prospects are discussed in Sec. 4. Finally, main conclusions are presented in Sec. 5.

2. Alpha-particle imaging detector based on gaseous micro-TPC

A new alpha-particle detector was developed based on a gaseous micro-TPC upgraded from the NEWAGE-0.3a detector [14] which was used to search for dark matter from September, 2008 to January, 2013. The detector consisted of the micro-TPC using a low-α μ-PIC as readout, a gas circulation system, and electronics, as shown in Fig.1. The TPC was enclosed in a stainless-steel vessel for the gas seal during the measurement.

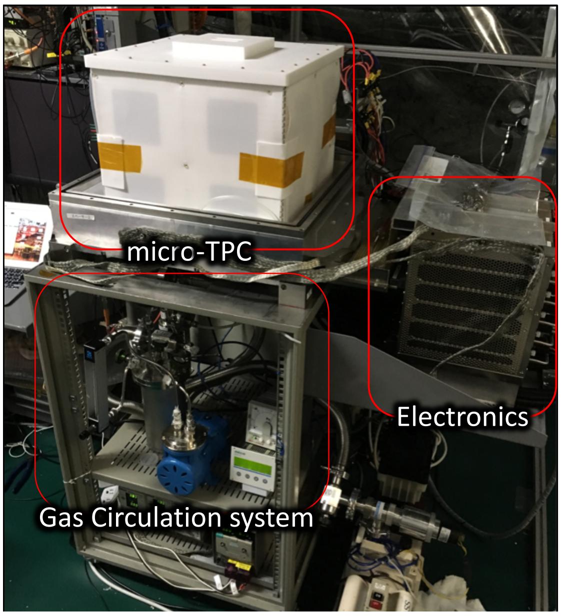

Fig. 1: Photograph of the experimental setup. The detector system is composed of a micro-TPC, a gas circulation system, and electronics. The stainless-steel vessel is uncovered so that the outer view of the TPC field cage can be viewed.

2.1. Setup and configuration

Figure 2 shows a schematic view of the detector, where the gas volume is (35 cm $\times$ 35 cm) $\times$ 31 cm. The detector was placed underground at the Kamioka facility in the Institute for Cosmic Ray Research, Japan. An oxygen-free copper plate with a surface electro-polished to a roughness of 0.4 μm and a size of (35 cm $\times$ 35 cm) $\times$ 0.1 cm was used as the drift plate. The drift plate had an opening with a size of 9.5 cm $\times$ 9.5 cm as a sample window. A copper mesh made of 1-mm-ϕ wire in 1-cm pitch (aperture ratio of 0.81) was set on the drift plate to hold the sample at the window area, as shown in Fig. 3. The electrons ionized by the alpha particles drift towards the μ-PIC with a vertical upward-pointing electric field E. CF_4 gas (TOMOE SHOKAI Co.LTD, 5N grade: a purity of 99.999% or more), which was also used in the NEWAGE-0.3a, was used because of the low diffusion properties. The pressure was set at 0.2 bar as a result of the optimization between the expected track length and the detector stability. The track length was expected to be longer, which improved the tracking performance when the gas pressures were low, while the discharge rate of the μ-PIC increased. The range of 5 MeV alpha particle is $\sim$8 cm in 0.2 bar CF_4 gas, which would provide a reasonable detection efficiency considering the detector size. The electric field in the drift volume, $E = 0.4\,\mathrm{kV/cm/bar}$, was formed by supplying a negative voltage of 2.5 kV and placing field-shaping patterns with chain resistors every centimeter [15]. The drift velocity was 7.4 ± 0.1 cm/μs. The μ-PIC anode was connected to +550 V. The typical gas gain of μ-PIC was 10^3 at $\sim$ 500 V.

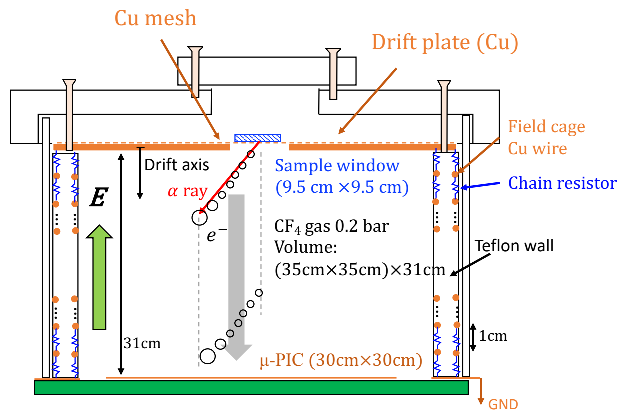

Fig. 2: Schematic cross section of detector setup. Sample window size is 9.5 cm × 9.5 cm. Electric field is formed by a drift plate biased at -2.5 kV and copper wires with 1 cm pitch connecting with chain registers.

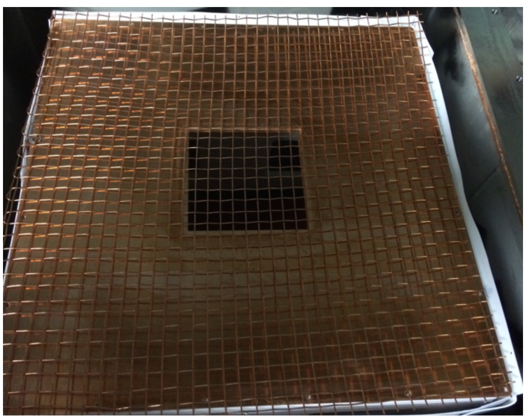

Fig. 3: Drift plate with a sample window (hole size is 9.5 cm × 9.5 cm) and copper support mesh.

2.2. Low-α μ-PIC

The background study for the direction-sensitive dark matter search suggests that μ-PIC has radioactive impurities of ^{238}U and ^{232}Th which emit alpha particles [5]. A survey with a HPGe detector revealed that μ-PIC's glass cloth was the main background source, and so the impurities were removed. The polyimide with glass cloth in the μ-PIC was replaced with a new material of polyimide and epoxy. Details of the device with the new material, a low-α μ-PIC, will be described in Ref [16, 17].

2.3. Gas circulation system

A gas circulation system that uses activated charcoal pellets (Molsievon, X2M4/6M811) was developed for the suppression of radon background and a prevention of gain deterioration due to the outgassing. A pump (EMP, MX-808ST-S) and a needle-type flow-meter (KOFLOC, PK-1250) were used to flow the gas at a rate of ~ 500 cm^3/min. The gas pressure was monitored to ensure the stable operation of the circulation system, operating within $\pm 2\%$ for several weeks.

2.4. Electronics and trigger and data acquisition systems

The electronics for the μ-PIC readout consisted of amplifier-shaper discriminators [18] for 768 anode and 768 cathode signals and a position-encoding module [19] to reconstruct the hit pattern. A data acquisition system consisted of a memory board to record tracks and a flash analog-to-digital converter (ADC) for the energy measurement. The flash ADC with 100 MHz sampling recorded the sum signal of the cathode strips with a full time range of 12 μs. The anode sum signal issued the trigger. The trigger occurred when the electrons closest to the detection plane (indicated with the largest circle (e^-) in Fig. 2) reach the μ-PIC. Since the main purpose of the detector is the alpha particle detection from the sample, the emission position of the alpha particle in the anode-cathode plane was determined at the position most distant from the μ-PIC in the track (the smallest circle in Fig. 2).

3. Performance check

3.1. Alpha-particle source

A 10 cm × 10 cm copper plate with ^{210}Pb accumulated on the surface was used as an alpha-particle source for the energy calibration and energy-resolution measurement [13]. The source emits alpha particles with an energy of 5.3 MeV as a decay of ^{210}Po. The alpha-particle emission rate (hereinafter called the α rate) of the entire source plate was calibrated to be 1.49 ± 0.01 α s^{-1} for 4.8–5.8 MeV by using the Ultra-Lo 1800 [13].

3.2. Energy calibration

An energy calibration was conducted with the alpha-particle source (5.3 MeV). The event's energy was obtained by integrating the charge from the pulses registered by the ~~flush~~flash ADC. Thus spectra showed in this paper are presented in MeV. Figure 4 shows a typical energy spectrum of the alpha-particle source. The energy resolution was estimated to be 6.7% (1σ) for 5.3 MeV, which is ~~worse than~~not as good as the Ultra-Lo 1800 resolution of 4.7% (1σ) for 5.3 MeV. This deterioration was thought to be due to the gain variation of the μ-PIC detection area.

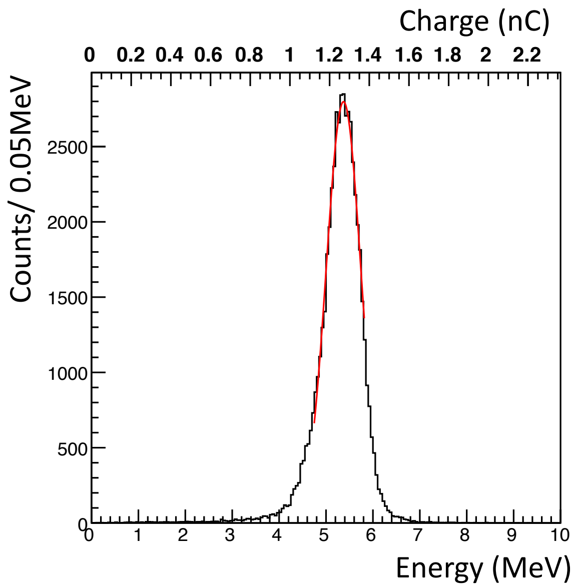

Fig. 4: Energy spectrum for alpha particles from ^{210}Po (5.3 MeV). Red line is a fit result with a Gaussian.

3.3. Event reconstruction

Figure 5 shows a typical event display with the tracks and flash ADC waveform data for alpha-particle emission from ^{210}Po. The hit points were determined based on coincidence of anode and cathode detections. Figure 5 (c) shows the anode-cathode plane for the track. The open circles correspond to hits registered in data. The red solid line is a linear fit result. The dashed line represents the edge of the sample window. The solid blue point is the emission point of the alpha particle. The scheme of the determination of the emission point, or the track sense, is explained in Sec. 3.4. Figure 5 (a) and (d) show anode- and cathode-drift planes, respectively. The drift coordinate is converted from the timing and is set to zero base, which corresponds to the drift-plate position. Figure 5 (b) shows a flash ADC waveform.

The track angles were determined on the anode-cathode, anode-drift, and cathode-drift planes. These angles were determined with a common fitting algorithm. First, the weighted means of the hit points $(x_{\rm w}, y_{\rm w})$ were defined as

$$\begin{pmatrix} x_{\rm w} \\ y_{\rm w} \end{pmatrix} = \frac{1}{n}\sum_{j=0}^{n} \begin{pmatrix} x_j \\ y_j \end{pmatrix}, \tag{1}$$

where x_j and y_j are the measured hit points and n is the number of points. Next, the track was shifted and rotated through the angle θ as follows

$$\begin{pmatrix} x'_j \\ y'_j \end{pmatrix} = \begin{pmatrix} \cos\theta & -\sin\theta \\ \sin\theta & \cos\theta \end{pmatrix} \begin{pmatrix} x_j - x_{\rm w} \\ y_j - y_{\rm w} \end{pmatrix}. \tag{2}$$

Here x'_j and y'_j are the points after the shift, the rotation angle θ were determined to minimize the quantity f, which is defined as

$$f(\theta) = \sum y'^2_j, \tag{3}$$

where this formula means a sum of the square of the distance between the rotated point and the x axis. This method has the advantage to determine the angle with no infinity pole at $\theta = 90^\circ$ (i.e. parallel to cathode strip (fitting in the anode-cathode plane) or drift axis (fitting in the anode-drift and cathode-drift plane)).

3.4. Track-sense determination

Backgrounds in low radioactivity alpha-particle detectors are in general alpha particles from the radon (radon-α) and materials of construction used in the detector (detector-α). The radon-α's are expected to be distributed uniformly in the gas volume with isotropic directions. The detector-α's are expected to have position and direction distributions specific to their sources. One of the main sources of the detector-α's is the μ-PIC so the directions of α's coming from this component are mostly

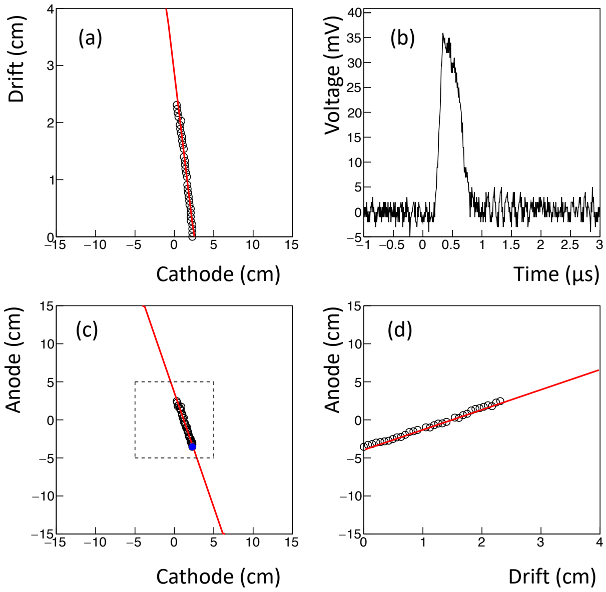

Fig. 5: Event display of an alpha particle from 210Po. (a) cathode-drift projection, (b) flash ADC waveform (c) cathode-anode projection, and (d) anode-drift projection are displayed. The drift coordinate is set to zero base corresponding to the drift plate position for the top of the track.

upward-oriented. Since the direction of alpha particles from the sample are downward, these detector-α's and half of the radon-α's can be rejected by the cut of upward-direction events.

The deposit energy per unit path length, dE/dx of an alpha particle with an initial energy over a few MeV, has a peak before stopping (Bragg peak). The number of electrons ionized by the alpha particle in the gas is proportional to dE/dx, and dE/dx along the track profile is projected onto the time evolution in the signal due to the mechanism of the TPC. This time profile was recorded as the waveform and thus the track sense (i.e., whether the track was upward or downward) can be determined from the waveform.

A parameter to determine the track sense is

$$F_{\mathrm{dwn}} = S_2/(S_1 + S_2), \tag{4}$$

where S_1 and S_2 are the time-integrated waveform before and after the peak. They defined as

$$S_1 = \int_{t_0}^{t_p} v(t)dt, \tag{5}$$

$$S_2 = \int_{t_p}^{t_1} v(t)dt. \tag{6}$$

Here, $t_0 = 0\ \mu$s, $t_1 = 1.5\ \mu$s, and t_p are the start, stop, and peak time, respectively, for the waveform shown in Fig. 5 (b). The t_p is determined as a time when the voltage is highest in the region between t_0 and t_1. Figure 6 (a) shows typical F_{dwn} distribution with the alpha-particle source, where most of the events are expected to be downward-oriented. The F_{dwn} values of the downward events are distributed around 0.7, as shown by the black-shaded histograms. Conversely, radon-α's have an isotropic direction, i.e., F_{dwn} has two components of upward- and downward-oriented, as shown by the red solid histogram, where the radon-α are background events in the sample test data, as explained later. The scale of the source-α was normalized to the radon-α peak of downward for clarity. Figure 6 (b) shows the efficiency related on F_{dwn} threshold for downward-(black solid) and upward-oriented (blue dashed). The selection efficiency of $F_{\mathrm{dwn}} > 0.5$ was estimated to be 0.964 ± 0.004 in the source-α spectrum while the radon background was reduced to half. The blue dashed histogram is a spectrum that subtracted the normalized source-α from the radon-α. The cut efficiency of the upward-oriented events ($F_{\mathrm{dwn}} \leq 0.5$) was estimated to be 0.85 ± 0.04. The energy dependence of F_{dwn} will be explained in Sec. 3.6.

3.5. Distribution of emission position

Since alpha particles are mainly emitted from the source, the top points of the alpha-particle tracks trace the shape of the radioactivity on the sample. Figures 7 (a) and 7 (b) show the anode–cathode projection distribution of the top and bottom of the alpha-particle tracks, respectively, where the top and bottom are defined as the zero and maximum drift coordinate, respectively, as shown in Fig. 5 (a) and 5 (d). The dashed line represents the edge of the drift-plate sample window. Comparing Fig. 7 (a) with Fig. 7 (b) clearly reveals the shape of the radioactivity.

The position resolution was evaluated along the four dashed lines in Fig. 7 (a). The number of events was projected onto the axis perpendicular to the lines and was fit with error functions as shown in Fig. 8. Figure 8 (a) and (b) represent the alpha-particle emission position projection to cathode and anode, respectively. The red lines are the fitting based on the error functions. As a result, the position resolution was determined to be 0.68 ± 0.14 cm (σ), where the error is a standard deviation in the four positions.

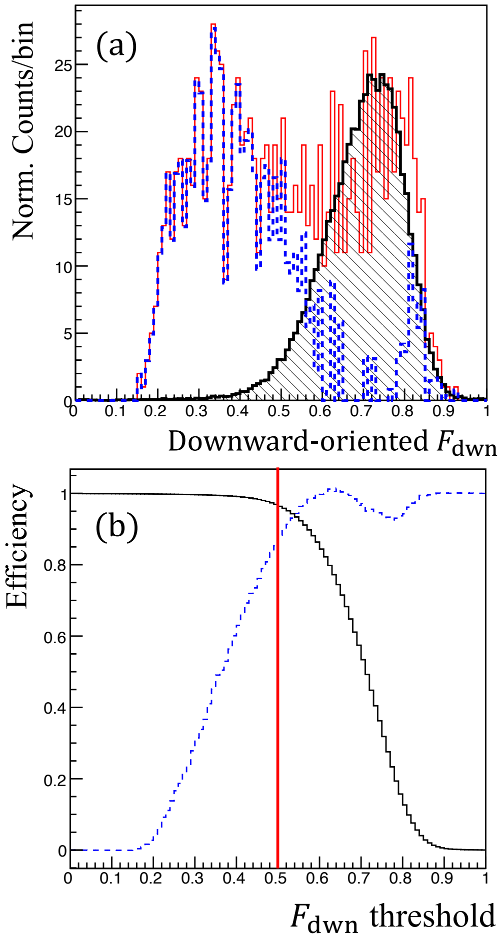

Fig. 6: (a) Downward-oriented distribution for source-α (black shade), radon-α (red solid), and a histogram made by subtracting the radon-α spectrum from the source-α one(blue dashed) (b) Detection efficiency for downward- (black solid) and rejection efficiency for upward-oriented (blue dashed) events as a function of F_{dwn} threshold.

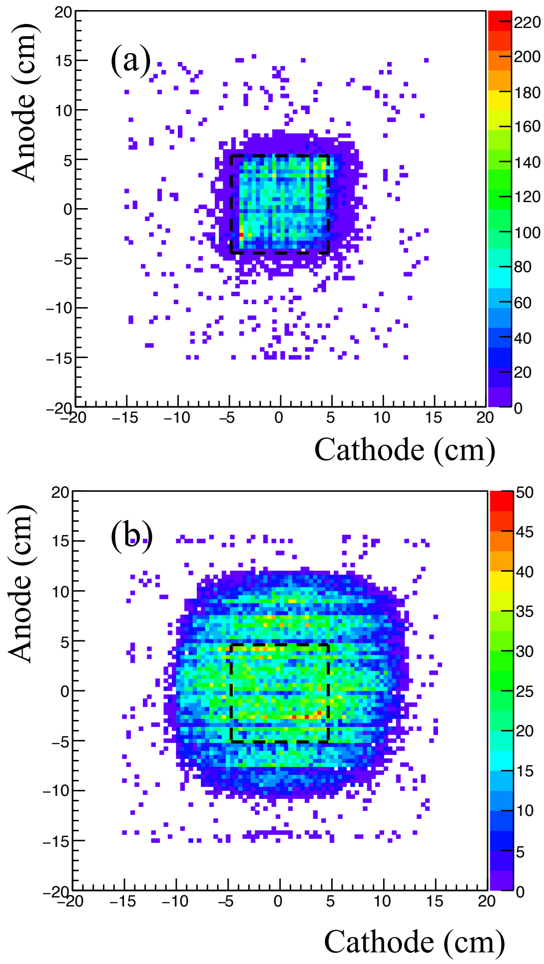

Fig. 7: Anode–cathode projection distributions of (a) top and (b) bottom of tracks for alpha particles emitted from the source. The dashed line is the edge of the sample window.

3.6. Detection and selection efficiency

To select good events for alpha particles from the sample, we use the following criteria: (C1) selection for events with good fitting tracks, (C2) cut for the upward-oriented events, and (C3) selection for events with emission points in the sample region.

For criterion C1, the ~~good~~best fit to track events was selected as $f_{\rm min}(\theta)/(n-1) < 0.02$ cm^2. It ~~is~~was determined as the best θ to minimize $f(\theta)/(n-1)$ at each plane, for both ~~track of electron~~tracking of electrons and α-ray. The electron track tends to be scattered, so $f_{\rm min}(\theta)/(n-1)$ ~~of electron~~for electrons is bigger than that of α-ray. Therefore, the upper limit of $f_{\rm min}(\theta)/(n-1)$ ~~makes to suppress~~serves to suppress electron-track events.

Criterion C2 rejects the upward-oriented tracks with > 3.5 MeV and $F_{\rm dwn} \leq 0.5$ because the determination efficiency depends on the energy. The upward- and downward-oriented tracks can be determined with 95% or more certainly at over 3.5 MeV. Note that this cut was applied for the events > 3.5 MeV, because the radon background, which was assumed to be the dominant background source, created the peak around 6 MeV and the contribution to the energy range below 3.5 MeV was limited.

For criterion C3, the source-α was selected within a region of ± 8 cm in both the anode and cathode. The cut condition was decided to cover both tails of the distribution (or ~~more~~$>4\sigma$) in Fig. 8 (a) and (b). The rate of radon-α in the selected region

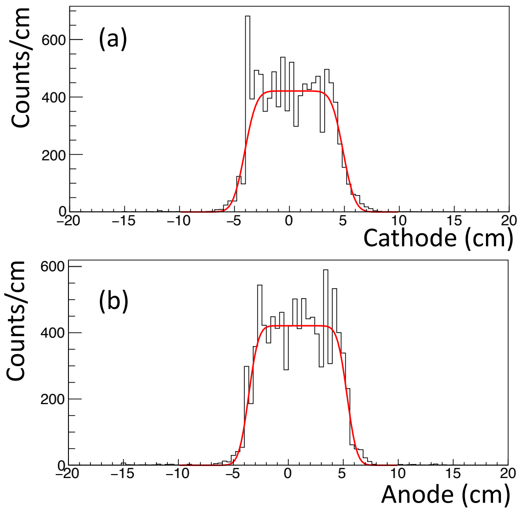

Fig. 8: Alpha-particle emission position projected to cathode (a) and anode (b). Red lines represent fitting with error functions.

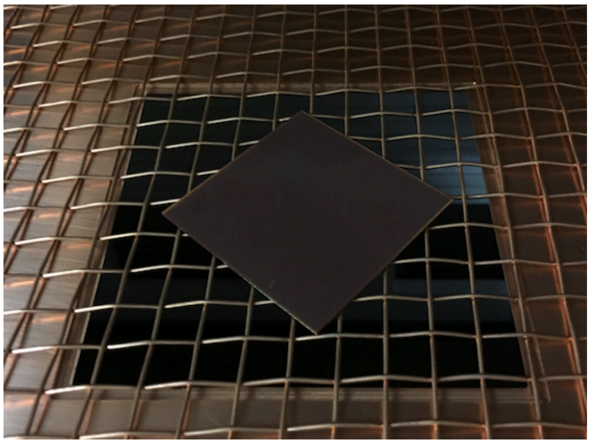

Fig. 9: Setup for a 5 cm × 5 cm piece of the standard μ-PIC as sample.

was around two orders of magnitude lower than the source-α rate, ~~considering negligible~~and considered negligible.

The selection efficiency for C1, C2, and C3 containing the detection efficiency was calculated to be $(2.17 \pm 0.29) \times 10^{-1}$ counts/α (the ratio of the count rate to the α rate of the source), where the error represents the systematic error of C1 to C3 selections and uncertainty of the source radioactivity is considered negligible.

3.7. Sample test and background estimate

3.7.1. Setup

A 5 cm × 5 cm piece of the standard μ-PIC whose α rate was known to be 0.28 ± 0.12 $\alpha/\text{cm}^2/\text{hr}$ in previous work [16] served as a sample and was inspected by using the detector. A photograph of the sample position over the setup mesh is shown in Fig. 9. The measurement live time was 75.85 hr.

3.7.2. Background in sample region

The α rate of the sample was estimated by subtracting the background rate. Considered background was mainly the radon-α. The detector measured both the α rates in the region of the sample and around the sample (outer region). The background rate could be determined from the α rate in the outer region. ~~Typically~~Recall, the upward and downward radon-α rates are same. The sample-α has mainly downward-oriented. Thus, the background rate could be estimated by the upward rate in the sample region and independently cross-checked by the upward rate in the outer region.

We checked the upward-oriented ($F_{\text{dwn}} \leq 0.5$) α rate in both regions because the alpha particles from a sample are typically emitted downward. Measured energy spectra are shown in Fig. 10. The red- and black-shaded histograms show the energy spectra inside and outside the sample region, respectively. These spectra are scaled by the selection efficiency. Both peaks are around 6 MeV and α rates are $(2.16^{+0.54}_{-0.35}) \times 10^{-2}$ (inside) and $(1.54^{+0.64}_{-0.40}) \times 10^{-2}$ $\alpha/\text{cm}^2/\text{hr}$ (outside). Therefore, the background condition inside the sample region is compatible at less than 1σ with the background condition outside the sample region. The alpha-particle energy spectrum is interpreted as the radon peaks at 5.5 MeV (^{222}Rn), 6.0 MeV (^{218}Po), and 7.7 MeV (^{214}Po).

The downward-oriented ($F_{\text{dwn}} > 0.5$) α rate outside the sample is $(1.58^{+0.29}_{-0.26}) \times 10^{-2}$ $\alpha/\text{cm}^2/\text{hr}$, as shown in the black-shaded spectrum of Fig. 11. In this work, the background rate was improved by one order of magnitude in comparison with that of our previous work [16]. The background reduction is attributed to the track-sense determination to reject upward-oriented alpha (for > 3.5 MeV) and the replacement of the low-α μ-PIC (for ≤ 3.5 MeV). In the energy region between 2.0 and 4.0 MeV, where most radon background is suppressed, the background rate is $(9.6^{+7.9}_{-5.6}) \times 10^{-4}$ $\alpha/\text{cm}^2/\text{hr}$.

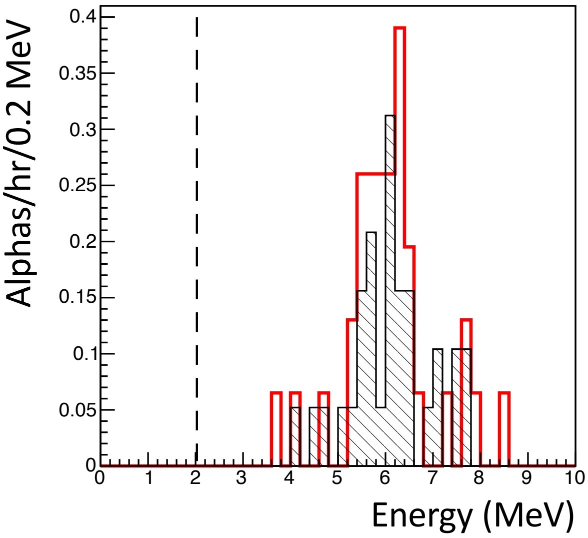

Fig. 10: Upward-oriented alpha-particle energy spectra inside (red) and outside (black shade) the sample region. The dashed line is the threshold of 2 MeV.

3.7.3. α rate of sample

Figure 12 shows the distribution of the top of the tracks for the sample, where the candidates are selected by the criteria C1 and C2. The regions ① and ② are defined as sample and background regions, respectively. The sample region corresponds to the sample window. The sample region is the inside of ± 5 cm of anode and cathode. The background region is the outside of the sample region and the inside of ± 7.5 cm of anode and cathode. The systematic uncertainty due to the setting of the background region is estimated by changing the outer bound by $\pm$ 0.5cm to be $\sim$ 0.5%. Figure 11 shows the energy spectra of downward-oriented alpha particles in the sample (red) and the background region (black shaded). The α rate of the sample was calculated to be $(3.57^{+0.35}_{-0.33}) \times 10^{-1}$ $\alpha/\mathrm{cm}^2/\mathrm{hr}$ ($>$ 2.0 MeV) by subtracting the background rate.

Here, the impurity of ^{232}Th and ^{238}U is estimated by comparing with a prediction of α rate spectrum in the simulation, where it mentions that the isotope in the material is assumed as only ^{232}Th or ^{238}U because of the continuous α rate spectrum. In the fit region between 2 and 10 MeV, the impurity of ^{232}Th or ^{238}U is estimated to be 6.0 ± 1.4 or 3.0 ± 0.7 ppm, respectively. The impurities of ^{232}Th and ^{238}U are measured to be 5.84 ± 0.03 and 2.31 ± 0.02 ppm, respectively, by using the HPGe detector with the measuring time of 308 hr. Although the error is huge because of the continuous energy spectrum, it is consistent with the prediction of prior measurement. In this sample test, it was demonstrated to observe the background alphas at the same time.

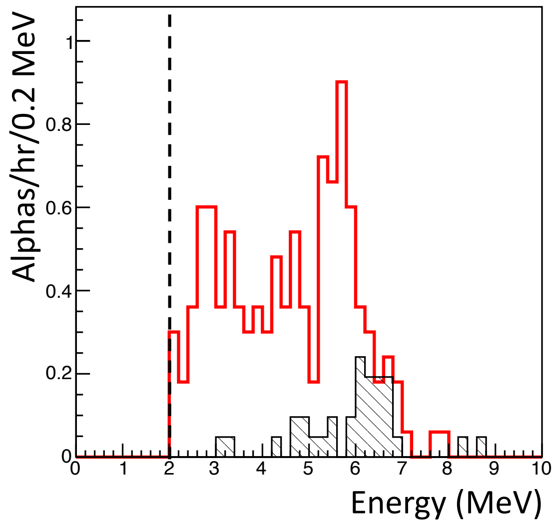

Fig. 11: Downward-oriented alpha-particle energy spectra in sample region (red) and background region (black shade). The dashed line is the threshold of 2 MeV.

4. Discussion

We begin by discussing the sensitivity for the energy between 2 and 9 MeV based on long-term measurements. In this energy range, the background is dominated by the radon-α's with $\sim$ $(1.58^{+0.29}_{-0.26}) \times 10^{-2}$ $\alpha/\mathrm{cm}^2/\mathrm{hr}$. The statistical error (σ) is expected to scale with the inverse of the square root of the measurement time (t) given as $\sigma \propto 1/\sqrt{t}$. In this work, the live time was only three days, and the statistical error was $\sigma \sim 3 \times 10^{-3} \alpha/\mathrm{cm}^2/\mathrm{hr}$. ~~With a measurement time of one month, the error of sample-α's was estimated to be $\sigma \sim 1 \times 10^{-3}$ $\alpha/\mathrm{cm}^2/\mathrm{hr}$. When the α rate ($\sigma \sim 1 \times 10^{-3}$ $\alpha/\mathrm{cm}^2/\mathrm{hr}$) as the same of the radon-α's ($\sigma \sim 1 \times 10^{-3}$ $\alpha/\mathrm{cm}^2/\mathrm{hr}$) was observed, the sum of squares of these σs for the sample and radon-α's would be expected to be a few 10^{-3} $\alpha/\mathrm{cm}^2/\mathrm{hr}$ as the measurement limit by subtraction with these α rates.~~ The sensitivity for a sample with a radioactivity much lower than the background rate is practically determined by the statistics of the background when the background can be subtracted. The expected statis-

	This work	HPGe detector
Sample volume (cm)	$(5 \times 5) \times 0.098$	$(5 \times 5) \times 2.47$
Sample weight (g)	6.8	169.5
Measureing time (hr)	75.85	308
Net α rate (α/cm^2/hr))	$(3.57^{+0.35}_{-0.33}) \times 10^{-1}$	—
^{232}Th impurities (ppm)	6.0 ± 1.4	5.84 ± 0.03
^{238}U impurities (ppm)	3.0 ± 0.7	2.31 ± 0.02

Table 1: Comparison of Screening result with this work and HPGe detector.

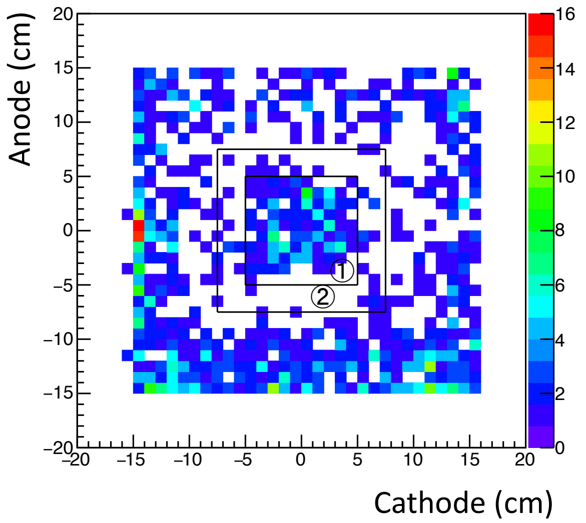

Fig. 12: Distribution of the top of downward-oriented alpha-particle track. The regions ① and ② are the sample and background regions, respectively.

tical errors of both the background and sample are 1×10^{-3} α/cm^2/hr with one month of measurement time. The statistical error of the subtracted event rate, or the detection sensitivity of the sample, is therefore expected to be a few $\times 10^{-3}$ α/cm^2/hr.

The edges region (anode $\sim \pm 15$ cm or cathode $\sim \pm 15$ cm) has a high rate of background, as shown in Fig. 12. These events have an energy and path-length dependence similar to that of the alpha particles. The alpha particles were mainly oriented upward and were emitted from outside the detection area, limited by the μ-PIC. As an impurity candidate, a piece of the printed circuit board (PCB) was inspected and the α rate was $(1.16 \pm 0.06) \times 10^{-1}$ α/cm^2/hr. Although the alpha-particle events could be rejected by the fiducial region cut, these impurities could be the radon sources (see Fig. 13). Therefore, as a next improvement, a material with less radiative impurities should be used for the PCB.

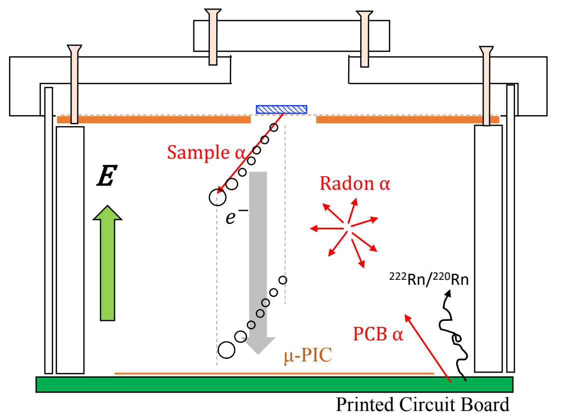

Fig. 13: Schematic cross section of background alpha particles in detector setup.

The goal for detector sensitivity is less than 10^{-4} α/cm^2/hr, which corresponds to measuring radioactive impurities at the ppb level. Here, this level was estimated as an assumption of ^{238}U or ^{232}Th in 1-mm-thick copper plate. We can potentially improve the background rate by using the cooled charcoal to suppress radon gas and using a material with less impurities such as polytetrafluoroethylene, polyimide, and polyetheretherketone without glass fibers. The goal for detector sensitivity is less than 10^{-4} α/cm^2/hr. We can potentially reduce the background rate by using the cooled charcoal to suppress radon gas and using a material with less impurities. Insulators such as polytetrafluoroethylene, polyimide, and polyetheretherketone, are in general low radioactive if we can use them without extra materials with relatively high radioactive like reinforcing glass-cloth.

A recent study reported that a cooled charcoal could suppress the radon by 99% in the argon gas [20]. A recent NEWAGE detector suppresses the radon to 1/50 by using cooled charcoal [5]. With these improvements, the detector would achieve to the goal of performance.

5. Conclusion

We developed a new alpha-particle imaging detector based on the gaseous micro-TPC. The measured energy resolution is 6.7% (σ) for 5.3 MeV alpha particles. The measured position resolution is 0.68 ± 0.14 cm. Based on a waveform analysis, the downward-oriented events' selection efficiency is 0.964 ± 0.004 and the cut efficiency of the upward-oriented events is 0.85 ± 0.04 at > 3.5 MeV. Also, a piece of the standard μ-PIC was measured as a sample, and the result is consistent with the one obtained by a measurement done with a HPGe detector. A measurement of the alpha particles from a sample and background was also established at the same time. A background rate near the radon-α ($(1.58^{+0.51}_{-0.42}) \times 10^{-2}$ $\alpha/\mathrm{cm}^2/\mathrm{hr}$) was achieved.

Acknowledgments

This work was supported by a Grant-in-Aid for Scientific Research on Innovative Areas, 26104004 and 26104008, from the Japan Society for the Promotion of Science in Japan. This work was supported by the joint research program of the Institute for Cosmic Ray Research (ICRR), the University of Tokyo. We thank Dr. Y. Nakano of the ICRR, University of Tokyo, Japan for providing us with a helium-gas leak detector.

References

[1] R Bernabei, et al., J. Phys. Conf. Ser. **1056** (2018) 012005.
[2] XENON Collaboration, Eur. Phys. J. **77** 881 (2017).
[3] D. S. Akerib, et al., Phys. Rev. Lett. **118** 021303 (2017).
[4] T. Tanimori, et al., Phys. Lett. B **578** (2004) 241.
[5] K. Nakamura, et al., Prog. Theo. Exp. Phys. (2015) 043F01.
[6] The GERDA Collaboration, Nature **544** (2017) 47.
[7] A. Gando, et al., Phys. Rev. Lett. **117** 082503 (2016).
[8] D. S. Leonard, et al., Nucl. Instr. Meth. A **871** (2017) 169.
[9] N. Abgrall, et al., Nucl. Instr. Meth. A **828** (2016) 22.
[10] R. Arnold, et al., Eur. Phys. J. C **78** (2018) 821.
[11] R. Arnold, et al., PRL **119**, 041801 (2017).
[12] A. S. Barabash, et al., JINST **12** (2017) P06002.
[13] K. Abe, et al., Nucl. Instr. Meth. A **884** (2018) 157.
[14] K. Miuchi, et al., Phys. Lett. B **686** (2010).
[15] K. Miuchi, et al., Phys. Lett. B **654** (2007) 58.
[16] T. Hashimoto, et al., AIP Conf. Proc. **1921**, 070001 (2018).
[17] T. Hashimoto, et al., in preparation.
[18] R. Orito, et al., IEEE Trans. Nucl. Scie. **51**, 4 (2004) 1337.
[19] H. Kubo, et al., Nucl. Instr. Meth. A **513** (2003) 93.
[20] M. Ikeda, et al., Radioisotopes, **59**, (2010) 29.

***Declaration of Interest Statement**

Declaration of interests

☑ The authors declare that they have no known competing financial interests or personal relationships that could have appeared to influence the work reported in this paper.

☐The authors declare the following financial interests/personal relationships which may be considered as potential competing interests: